Energy Conversion and Management 255 (2022) 115263

Contents lists available at ScienceDirect

Energy Conversion and Management

journal homepage: www.elsevier.com/locate/enconman

Adoption of the $CO_2 + SO_2$ mixture as working fluid for transcritical cycles: A thermodynamic assessment with optimized equation of state

Ettore Morosini [a,*], Abubakr Ayub [b], Gioele di Marcoberardino [b], Costante Mario Invernizzi [b], Paolo Iora [b], Giampaolo Manzolini [a]

[a] Politecnico di Milano, Dipartimento di Energia, Via Lambruschini 4, Milano 20156, Italy
[b] Università degli Studi di Brescia, Dipartimento di Ingegneria Meccanica ed Industriale, via Branze, 38, Brescia 25123, Italy

ARTICLE INFO

Keywords:
CO_2 mixtures
Transcritical cycles
CSP applications
Equations of state
Power cycle analysis

ABSTRACT

This paper focuses on the use of the $CO_2 + SO_2$ binary mixture as innovative working fluid for closed transcritical power cycles with a minimum temperature above 50 °C. Starting from a literature review of the available experimental data on the mixture, the PC-SAFT EoS is identified as a suitable model to characterize the mixture behavior. Once the proper thermodynamic model is selected for this mixture, a comparison between the innovative transcritical cycle and the sCO_2 cycle is proposed for various plant layouts in order to find out the advantages of the innovative mixture. The analysis is presented fixing the cycle maximum temperature at 700 °C and the maximum pressure at 250 bar: the results depict an increment in cycle electric efficiency and cycle specific work, along with a lower temperature of heat introduction in the cycle for any considered configuration of transcritical $CO_2 + SO_2$ cycle, when compared to pure sCO_2.

An economic analysis of the power block is then performed to support the selection of the innovative working fluid. Two of the most promising plant layouts are evidenced: the recompression layout is selected for highly efficient power blocks, while the dual recuperated layout works effectively in applications characterized by higher hot source exploitation. The recompression layout adopting the $CO_2 + SO_2$ mixture presents a power block electric efficiency of 48.67% (2.33% higher than the respective sCO_2 cycle) and a reduction of the power block CAPEX from 1160 $/kW$_{el}$ to 1000 $/kW$_{el}$ when compared to the sCO2 configuration for a 100MW$_{el}$ size, while the dual recuperated layout exploiting the $CO_2 + SO_2$ mixture shows a power block electric efficiency of 39.58% (0.69% above the same sCO_2 cycle), a decrease of power block CAPEX from 795 $/kW$_{el}$ to 718 $/kW$_{el}$ and 70 °C of additional heat recovery from the hot source with respect to the analogous sCO_2 cycle.

1. Introduction

Among the many renewable energy technologies, concentrated solar power (CSP) is one of the most promising due to the adoption of thermal energy storage systems that allow a flexible electric load regulation. Unfortunately, nowadays, if compared to other non-dispatchable technologies (i.e. PV, wind) it is far from being competitive from economic point of view [1].

Most of the recent studies on CSP plants design and optimization focused on the development of advanced thermodynamic cycles that reduce the LCOE by increasing the conversion efficiency of heat into electricity and reducing the cost of the power block. This goal can be achieved both adopting innovative working fluids, different from steam, and increasing the maximum temperature of the power cycle. Considering the current state of the art of power cycles based on this technology, molten salts are used as HTF (with maximum temperatures of 565 °C) and the steam Rankine cycle is employed in the power block [2]. The typical steam cycle used in CSP applications exploits a significant number of bleedings to increase the feedwater temperature in order to couple the cycle characteristics with the one of the hot source, resulting in an high specific costs of the power block [3]. It is also characterized by a high thermal inertia that promotes slow transients and it exploits condensation at pressures below the atmospheric one. To overcome these problems, the supercritical carbon dioxide (sCO_2) Brayton power cycles has been studied as valid alternative to steam cycles, due to a higher cycle efficiency at medium to high maximum temperatures (500 to 700 °C) along with compact size and a simpler layout of the power cycle [4]. Moreover, studies have confirmed the

* Corresponding author.
E-mail address: ettore.morosini@polimi.it (E. Morosini).

https://doi.org/10.1016/j.enconman.2022.115263
Received 11 October 2021; Received in revised form 23 December 2021; Accepted 15 January 2022
Available online 10 February 2022

lower costs and higher performances of sCO_2 cycles compared to the Rankine cycle if adopted in waste heat recovery cycles [5], gas turbine bottom cycles [6] and nuclear [7] applications. Due to these favorable characteristics, different projects have studied how to improve the performance of CSP power plant by replacing traditional steam Rankine cycles with sCO_2 cycle. The U.S. Department of energy (DOE) launched the Sun Shot program in 2011 with the aim of reducing the cost of CSP power plants by adopting sCO_2 cycles [8]. Another project, in China, works on the retrofit of a traditional 10 MW CSP power plant with the sCO_2 cycle [9].

The majority of the published research on sCO_2 cycles considers the compressor inlet conditions close to the critical point (i.e. 31 °C and 74 bars) in order to take advantage of the higher CO_2 density in that region, a condition that minimizes the compression work. On the other hand, this condition would lead to a considerable difference in the specific heat of CO_2 between the low- and the high-pressure side of the recuperators, increasing the irreversibility during the heat exchange recuperative process. To overcome this problem, it is possible to adopt the recompression cycle as power block configuration, or any other similar variations in the power block layout as the split cycle suggested by Dostal *et* al [7] and Crespi *et* al [10], among the many. Nevertheless, the cycle efficiency of sCO_2 cycles drops when the compressor inlet temperature increases: this condition occurs when a cooling medium at low temperature (i.e. below 20 °C) is not available to cool the sCO_2 flow close to the critical temperature in the heat rejection unit of the power cycle [11]. Notably, in typical CSP locations where the ambient temperature can be up to 30 °C or 40 °C during peak summer days, the adoption of an air-cooled heat rejection unit is usually the only configuration for the power block. At these ambient conditions, the compressor inlet temperature rises and higher compressibility factors of CO_2 during the compression step lead to a growth in compression work and a drop in cycle efficiency [12].

To address this issue, Lin *et* al [13] modified the configuration of the sCO_2 recompression cycle which proved to be less sensitive to increments in compressor inlet temperature; the modification proposed yielded 1.92% of cycle efficiency increase with respect to typical sCO_2 recompression cycle at compressor inlet temperature of 50 °C.

An alternative to the modification of the plant layout to increase the cycle efficiency can be the adoption of CO_2 based binary mixtures, substituting pure CO_2 as working fluid for the power block: the rationale of this approach is to increase the critical temperature of the working fluid in the range between 70 °C and 120 °C by adding a certain amount of a specific dopant, hence turning the supercritical cycle into a transcritical one. Therefore, it would become possible to use a pump instead of a compressor in the compression process. In recent years, some works explored CO_2 mixtures as working fluids for low grade heat recovery [14], medium to high grade heat recovery [15] and high temperature like nuclear application [16]. Liu *et* al [17] considered the CO_2 + cyclohexane, CO_2 + propane, CO_2 + butane, CO_2 + isobutane and CO_2 + H_2S mixtures as candidate working fluids and assessed the performance of the power cycle at different ambient temperatures. It was found that power cycles operating with CO_2-based binary mixtures yield better efficiencies under higher ambient temperature compared to sCO_2 Brayton cycles, even though no analysis of the thermochemical stability of the selected additives at turbine inlet temperatures (i.e. 550 °C) was carried out. Guo *et* al [18] recommended CO_2 + Xenon as suitable mixture to enhance the cycle efficiency of sCO_2 Brayton cycle integrated with a solar tower CSP plant: nevertheless, this solution does not turn the supercritical cycle into a transcritical one, maintaining the compression in gaseous phase. CO_2 + Toluene and CO_2 + R32 mixtures have also been proved good candidates to achieve a higher cycle performance than pure sCO_2 cycles in hot climates [19], even if their thermal stability is limited to temperatures well below 550 °C. In addition, Rath *et* al [20] proposed a multi-fluid mixture models to accurately calculate the properties of 135 CO_2 mixtures and used these mixtures as working fluids in power cycles: the study focuses on screening of most suitable CO_2 mixtures to increase the cycle efficiency of traditional sCO_2 cycle, but it overlooked the significance of the thermal stability of additives at cycle maximum temperature of 500 °C.

The concept of the adoption of binary CO_2 mixtures for closed cycles is also proposed in the SCARABEUS project, an EU Horizon 2020 project which aims at improving the cycle efficiency and reducing the LCOE of CSP plants adopting CO_2 blends as working fluids in power block [21]. With respect to the various previous investigations already mentioned about CO_2 mixtures, the SCARABEUS project is interested in finding mixtures to be used only for transcritical cycles (where a condenser is adopted as heat rejection unit and a pump is adopted in the compression step), and a considerable attention to the thermal stability of the dopants is paid, considering only CO_2-based mixtures thermally stable at least up to 550 °C.

Within this new perspective Bonalumi *et* al [22] considered $TiCl_4$ as possible dopant, finding a 5% gain in cycle efficiency with a simple recuperative cycle and a 3% gain in cycle efficiency with a recompressed cycle using CO_2 + $TiCl_4$ as working fluid with respect to sCO_2 at cycle maximum temperature of 550 °C. Manzolini *et* al investigated the CO_2 + $TiCl_4$ and CO_2 + N_2O_4 mixtures as working fluid in simple recuperative cycles for a CSP power plant located in Las Vegas (US) and Seville (Spain). The studies demonstrated that the selected CO_2 blends outperforms the sCO_2 cycle and conventional steam Rankine cycle in terms of cycle efficiency [23] and LCOE [21].

Nevertheless, the studies previously mentioned adopted simplified models for the calculation of the mixture thermodynamic properties (as the standard Peng Robinson equation of state) which were calibrated only on few experimental VLE (vapor liquid equilibrium) data: as a matter of fact, to improve the accuracy of these models, a wider validation of the variables computed by the equations of state (EoS) against the experimental data is required.

However, in the selection of the most suitable CO_2-based mixture, the cycle efficiency is not the only important parameter to consider: some other aspects related to the toxicity and the flammabilty limits of the working fluid are crucial. Under this perspective, the mixture CO_2 + C_6F_6 has been studied in the SCARABEUS project and identified as one of the most promising CO_2-based mixture for transcritical cycles. Di Marcoberardino *et* al [24] proposed the analysis of the simple recuperative transcritical cycle employing this mixture: the emphasis of this work is on the sensitivity analysis of the resulting performances varying the equation of state used to model the thermodynamic variables of the working fluid. The authors found that the choice of the EoS is of paramount importance in the cycle modeling, as the final results are influenced by the EoS adopted: for this reason, a detailed knowledge of the mixture behavior is necessary.

In this work the thermodynamic properties of the CO_2 mixture which adopt sulfur dioxide (SO_2) as dopant are computed and compared to experimental data. In particular, the performance of the CO_2 + SO_2 blend as working fluid in power blocks is assessed with both thermodynamics and economic indicators assuming a cycle maximum temperature of 700 °C. The thermodynamic behavior of the mixture is modelled using three well-known EoS calibrated on available experimental VLE data, while the selection of the most suitable EoS is based on the comparison of some computed thermodynamic variables (densities, speed of sound, residual specific heat and inversion curves) with available experimental data. Since the CO_2 + SO_2 mixture has been already studied as a mixture of interest in the carbon capture and storage field, a larger amount of experimental data are available with respect the CO_2 + C_6F_6 mixture, enabling a more detailed optimization procedure of the EoS on experimental data.

Sulfur dioxide is selected as a promising working fluid due to its thermal stability even at high temperatures: as a matter of fact, it is usually produced during combustion of coal in coal-fired power plants and can be produced during volcanic eruptions, two conditions where the exhaust gases reach very high temperatures. From a molecular point of view, it presents two strong S-O double bond (having 522 kJ/mol as

average bond energy), a chemical bond considered stronger than the C-F bond (which has 485 kJ/mol as bond energy). For these reasons, in this work, the $CO_2 + SO_2$ mixture is investigated up to 700 °C, where the $CO_2 + C_6F_6$ is not considered thermally stable. In addition, sulfur dioxide is not a flammable gas, it does not react with air, water nor CO_2 and its ozone depletion potential (ODP) is completely negligible. [25]. Further experimental tests are however required to verify the chemical compatibility of SO_2 with the typical materials used in power block components (stainless steel or Inconel). Finally, the presence of sulfur make this compound toxic (with toxicity level of 3 according to NFPA [26]), representing the only major drawback in the adoption of this dopant. Nevertheless, as working fluid for closed cycles in CSP application, the adoption of $CO_2 + SO_2$ mixture should not pose significant threats: the locations selected for CSP plant are typically arid and desertic region, the leaks from the cycle are normally very limited and the power block is placed in a confined and controlled environment with constant ventilation.

The scope of this paper is the characterization of the thermodynamic behavior of the $CO_2 + SO_2$ mixture adopted in power cycles as working fluid. Some of the most important key performance indicators from the thermodynamic perspective will be computed, and the overall cost analysis of power cycles operating with the $CO_2 + SO_2$ blend will be compared to the one representative of the sCO_2 cycle.

The analysis covers the following aspects:

- Optimization of EoS using experimental VLE data
- Selection of the most promising EoS by comparing the predictive capability of different EoS
- Thermodynamic and economic assessment of transcritical power cycle with $CO_2 + SO_2$ mixture as working fluid

As per knowledge of the authors, many studies in literature do not consider the aspect of accuracy of the EoS in calculating the thermodynamic behavior of CO_2 mixtures.

2. Thermodynamic properties of $CO_2 + SO_2$ mixture

2.1. Determination of binary interaction parameter for EoS

The first step required for the thermodynamic modeling of CO_2 mixtures is represented by an accurate calculation of thermodynamic properties in the temperature and pressure range of interest.

Among the several EoS which can be adopted, three EoS have been selected and compared: 1) the standard Peng Robinson EoS (PR) with soave alpha function [27], 2) the PC-SAFT EoS [28], 3) the REFPROP inbuilt EoS (extended GERG-2008 EoS [29]). The selected equations of state cover a wide spectrum of options: PR is an extensively adopted cubic EoS (thanks to the limited amount of required input data and its accuracy in VLE calculations), PC-SAFT is very versatile and proved to be accurate for CO_2 mixtures and REFPROP (which is considered as a reference tool in many studies to predict properties of pure fluids and mixtures) can rely on a specific formulation of an Helmholtz EoS optimized on this mixture. As previously mentioned, most of the literature studies on CO_2 mixtures used as working fluid in closed cycles did not consider the evaluation of EoS performances, not identifying the most accurate property model. This work aims at filling this gap by comparing the properties predicted by three EoS and recommending the one which demonstrates the minimum deviations from experimental data.

The Peng-Robinson EoS, used in numerous studies in past, only requires the critical point temperature and pressure (T_{cr}, P_{cr}), the acentric factor (ω) and the molecular weight (MW) of each pure component. In addition, an optional binary interaction parameter (k_{ij}) can be used to completely describe the VLE properties of the selected binary mixture.

The PC-SAFT EoS is based on the perturbation theory, according to which a molecule is modeled as a chain molecule with freely joined spheres. This EoS requires three pure component parameters known as segment number (m), segment diameter (σ) and segment-segment interaction energy (ε/k). An additional binary interaction parameter (kij) can be included, as for the PR EoS. All the required parameters for the PR and PC-SAFT EoS are reported in Table 1 for both CO_2 and SO_2.

Table 1
Pure component parameters required in Peng Robinson EoS and PC-SAFT EoS.

Pure fluid	T_{cr} (°C)	P_{cr} (bar)	ω	MW	PC-SAFT EoS parameters		
					m	σ	ε/k
CO_2	31	73.8	0.2236	44.01	2.569	2.564	−121.05
SO_2	157.6	78.8	0.2454	64.06	2.861	2.683	−67.80

The last EoS considered is the extended form of GERG-2008 EoS proposed by Neumann et al [29] to predict thermodynamic properties of some CO_2 rich mixtures, such as CO2 + Ar [30]. It involves four parameters ($\beta_{T,ij}$, $\beta_{V,ij}$, $\gamma_{T,ij}$, $\gamma_{V,ij}$) to compute temperature and density reducing functions.

The values of these parameters, presented in Table 2, are determined by curve fitting with available experimental data and available within the REFPROP database. The GERG-2008 EoS optimized with the binary interaction parameters relative to the $CO_2 + SO_2$ mixture by Neumann et al and implemented in the software REFPROP will be presented, in the next figures and tables, in the abbreviated form “Refprop EoS”.

In this work the performance of sCO2 cycles will also be presented: for pure CO_2 the reference EoS known as Span and Wagner EoS [31] is used, since it covers a wide range of temperature and pressure and it is the most accurate EoS available for this pure fluid [32].

The procedure developed in this work for the selection of the optimal EoS can be summarized in the following three steps:

- PR and PC-SAFT are calibrated on sets of VLE experimental data (P,x, y) available in literature (for the GERG-2008 EoS the binary parameters are already optimized) [33];
- The accuracy of the three equations of state is evaluated with reference to experimental VLE data ($P-\rho-T$), densities, speed of sounds, pseudo experimental residual heat capacities and Joule Thompson inversion curves available in literature [34,35] for the $CO_2 + SO_2$ mixture.
- An overall index to identify the most accurate EoS is proposed and used.

In this section the first of the three steps will be developed, as the different equations of state presented are optimized using experimental VLE data available in literature. The rationale is to compare the predictive capability of different EoS and identify the most suitable one for the $CO_2 + SO_2$ mixture.

The selected PR EoS and PC-SAFT EoS are non-predictive, as they need to be calibrated using available experimental data: VLE data are usually used for this procedure in literature. The typical approach well known in literature involves fitting the EoS on the experimental VLE data and finding the optimum value of binary interaction parameter (BIP). In order to adopt this methodology, the experimental bubble pressure and dew composition given by Coquelet *et* al [33] are fitted using the selected EoS. Coquelet’s work was selected as its data covers a wide range of operating temperatures (-10 °C to 60 °C) and compositions, as the approach to determine binary interaction parameters on the basis of isothermal (P,x,y) VLE data is the most common.

The accuracy of each EoS is assessed by computing the mean absolute percentage error (MAPE), an index that indicates the deviation

Table 2
Binary parameters for REFPROP v10 inbuilt EoS.

CO_2 mixture	$\beta_{T,ij}$	$\beta_{V,ij}$	$\gamma_{T,ij}$	$\gamma_{V,ij}$
$CO_2 + SO_2$	1.0201	0.8899	1.0080	1.0058

Table 3
MAPE for different EoS in the VLE calculations with respect to experimental data reported in [33]

Equation of state	Binary parameter	MAPE of P_{bub}			MAPE of y_{dew}		
		−10 °C	60 °C	Average	−10 °C	60 °C	Average
PR EoS	0.0242	1.4%	0.6%	1.0%	0.3%	0.8%	0.5%
PC-SAFT	0.0121	0.8%	1.1%	0.9%	0.7%	1.7%	1.2%
REFPROP	Table 2	2.0%	1.3%	1.7%	0.5%	1.7%	1.1%

between the computed value by the EoS and the experimental data, presented in Eq. (1). For this optimization the MAPE of bubble pressures (P_{bub}) and dew composition (y_{dew}) are computed and shown in Table 3.

$$MAPE_X[\%] = \frac{1}{N}\sum_{i=1}^{N}\left|\frac{X_{EoS} - X_{experimental}}{X_{experimental}}\right| x100 \quad (1)$$

The result of the regression analysis returns the optimized value of k_{ij} that best fits the selected EoS. Aspen Plus v.11 [36] is used to perform this regression analysis. As previously mentioned, no optimization was carried out for the REFPROP EoS, since the EoS already includes binary interaction parameters. The optimized value of k_{ij} for all EoS calculated in this study are reported in Table 3. The graphical representation of experimental VLE data and fitted EoS on P-xy plane is shown in Fig. 1.

2.2. Equations of state validation and comparison of the results

Once the selected EoS have been calibrated on the mixture real VLE behavior, they are also evaluated on different sets of experimental data available in literature. In order to perform this analysis, VLE data (in $P-\rho-T$ form) and densities from Gimeno *et* al [34] are considered along with densities, speed of sound, inversion curves and pseudo experimental residual specific heat from Nazeri et al [35].

The methodology proposed will evidence the EoS which reports the lower deviation from experimental data.

Fig. 2 and Fig. 3 show $P-\rho-T$ data, reported by Gimeno et al [34], compared to the modelled values from the three EoS. The corresponding MAPE in bubble and dew point properties for the three equations are shown in Table 4. All the selected EoS are reasonably accurate in predicting bubble and dew point pressures and densities. Comparing the densities computed, it must be noted that PR EoS shows a good agreement in bubble point densities if compared to the values from PC-SAFT and REFPROP. It must be pointed out that the prediction of the bubble point density is very relevant for the calculation of the compression step in a thermodynamic cycle, strongly affecting the cycle efficiency.

The graphical comparison of experimental liquid densities of the mixture from Gimeno et al and the computed values by the EoS for a CO_2 molar composition of 80% is illustrated in Fig. 4 and the corresponding MAPE for both the 80% and 90% molar CO_2 mixture are reported in Table 5. Among the three models, PC-SAFT EoS shows the best accuracy in predicting liquid densities of the mixture. In addition, a comparison with density data of Nazeri et al for 95% molar CO_2 mixture also reveals minimum deviations for the PC-SAFT and the REFPROP EoS, as presented in Table 6.

The same approach is developed with some calorimetric variables, comparing the values computed by the EoS and the reference experimental data from literature [34]. The considered variables include the speed of sound, the residual specific heat and the inversion curve of the mixture: their expressions are reported from Equation (2) to Equation (4). The inversion curve is a locus of thermodynamic conditions indicating where the residual enthalpy ($\Delta h_{residual} = \int_0^P v - T.\frac{\partial V}{\partial T} dP$) presents a minimum.

$$c = \sqrt{\frac{C_p}{C_v}\frac{dP}{d\rho}} \quad (2)$$

$$\Delta C_{p,residual} = -\int_0^P T\left(\left(\frac{\partial^2 v}{\partial T^2}\right)_P\right)_T dP \quad (3)$$

$$\frac{v}{T} = \frac{\partial v}{\partial T} \quad (4)$$

Fig. 5 and Fig. 6 compares the speed of sound and residual specific heat with experimental data, while the corresponding MAPE are reported in Table 7 and Table 8, respectively.

Considering the speed of sound in the liquid region for 80% molar CO_2 mixture, the comparison reveals a large MAPE, around 10%, corresponding to PR EoS. The PC-SAFT and REFPROP EoS have instead MAPE lower than 2% at all temperatures.

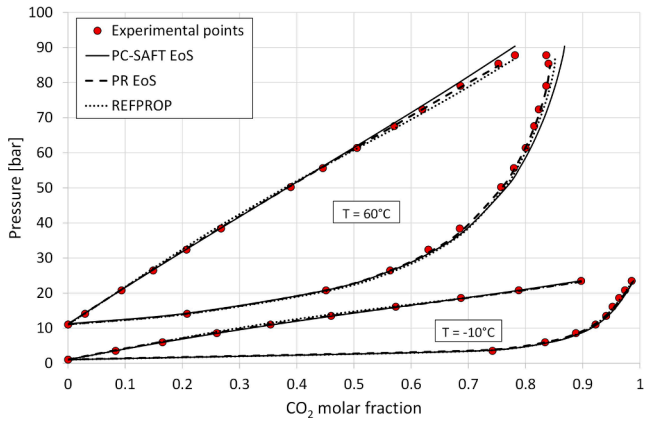

Fig. 1. Comparison of predicted VLE by the selected EoS with experimental data at two temperatures. Experimental points are taken from [33]

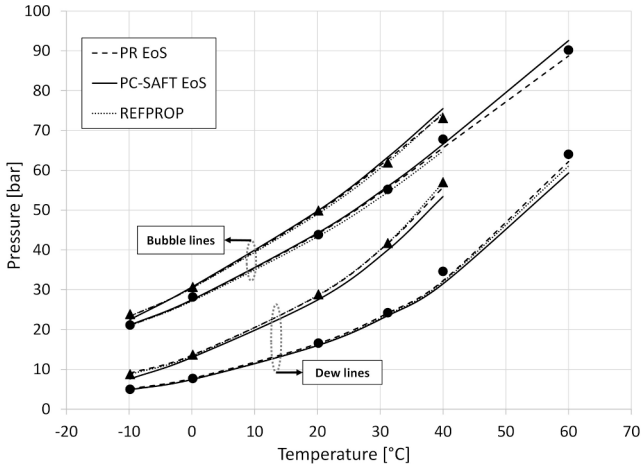

Fig. 2. Comparison of bubble and dew point pressures among three EoS and experimental data. Triangles show experimental points for 90% molar CO_2 mixture, Solid circles show experimental points for 80% molar CO_2 mixture from [34]

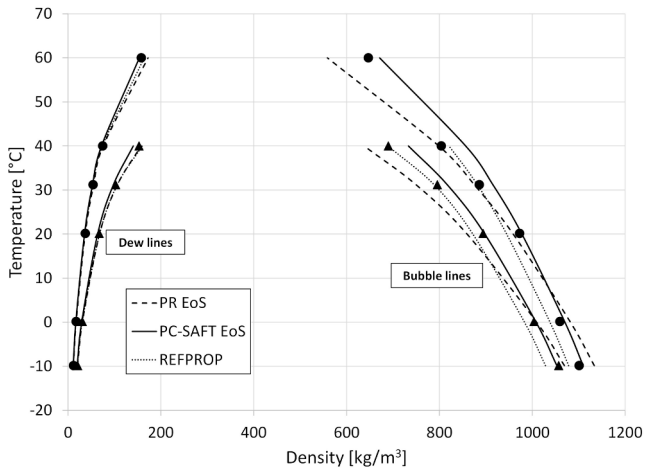

Fig. 3. Comparison of bubble and dew point densities among three EoS and experimental data. Triangles show experimental points for 90% CO_2 mixture, Solid circles show experimental points for 80% CO_2 mixture from [34]

Table 4
MAPE of predicted bubble point pressures and bubble point densities of CO_2 + SO_2 mixture with respect to experimental data from [34]

Equation of state	Molar Fraction	MAPE of bubble point		MAPE of dew point	
		Pressure	Density	Pressure	Density
PR EoS	80% CO_2	1.2%	3.7%	1.1%	2.4%
PC-SAFT		1.5%	2.6%	4.5%	3.7%
REFPROP		2.1%	1.9%	3.4%	2.5%
PR EoS	90% CO_2	1.2%	3.8%	1.3%	1.9%
PC-SAFT		2.3%	2.0%	6.6%	5.4%
REFPROP		1.3%	1.7%	0.6%	2.7%

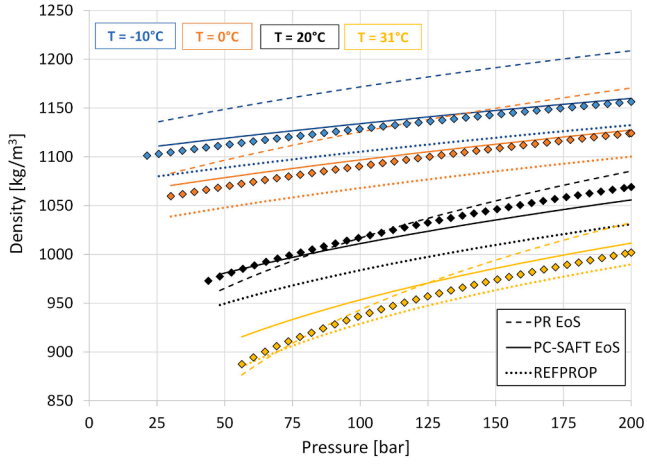

Fig. 4. Comparison of predicted densities with experimental densities in the liquid region for the CO_2 + SO_2 mixture (80% molar CO_2). Experimental densities (scatter points) are taken from [34]

Table 5
Mean absolute percentage error (MAPE) of predicted densities of CO_2 + SO_2 mixture with reference to experimental data from [34]

Equation of state	Molar fraction	MAPE of density			
		−10 °C	0 °C	20 °C	31 °C
PR	80% CO_2	4.2%	3.8%	1.1%	1.8%
PC-SAFT		1.4%	1.6%	1.3%	1.6%
REFPROP		2.7%	2.8%	2.8%	1.2%
PR	90% CO_2	3.3%	2.1%	1.4%	2.5%
PC-SAFT		1.2%	0.6%	0.7%	1.9%
REFPROP		2.9%	2.2%	2.1%	2.1%

Table 6
Mean absolute percentage error (MAPE) in predicted densities of CO_2 + SO_2 mixture with reference to experimental data from [35]

Equation of state	Molar fraction	MAPE of density					
		400 bar	350 bar	300 bar	250 bar	200 bar	150 bar
PR	95% CO_2	3.7%	3.1%	2.9%	2.7%	2.8%	2.7%
PC-SAFT		1.0%	1.1%	1.2%	1.3%	1.4%	1.1%
REFPROP		1.3%	1.2%	1.1%	1.0%	0.8%	1.1%

Finally, the Joule Thompson inversion curve for a single temperature (at 0 °C) and various mixture compositions is also computed and compared with the experimental data, reported in Fig. 7. The REFPROP and PC-SAFT EoS show good agreement with experimental inversion pressures compared to the PR EoS. Nevertheless, due to the limited number of experimental points and the single temperature reported, no MAPE is presented for these calculations. The interest in fitting the inversion curve with EoS used to model thermodynamic cycles lies in the characterization of the trend of enthalpies, a crucial step for the definition of the power balance and the efficiency of the cycle.

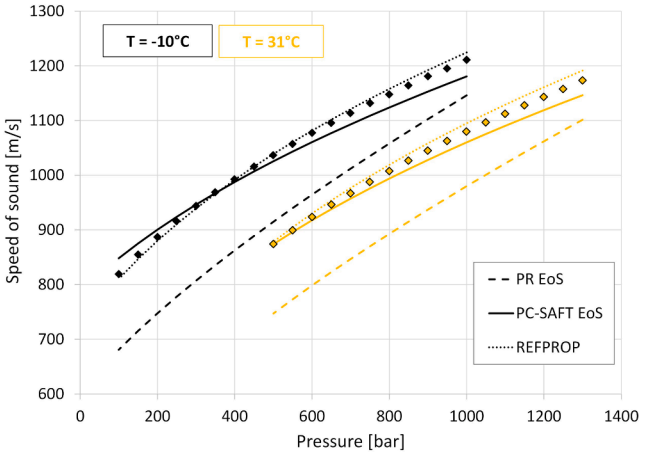

Fig. 5. Comparison of predicted speed of sound with experimental speed of sound of the CO_2 + SO_2 mixture (80%). Experimental values (scatter points) are taken from [34]

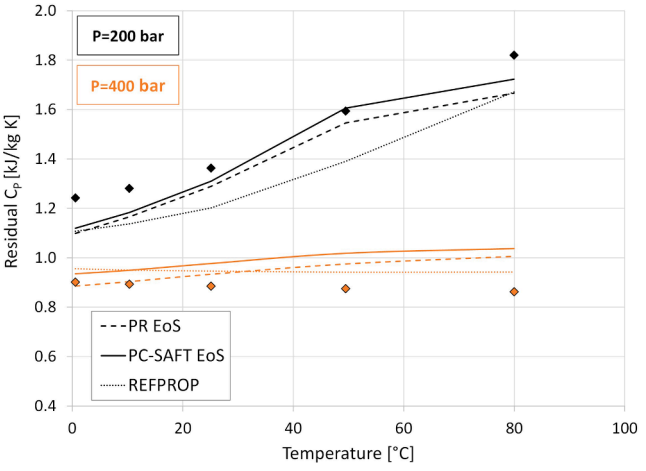

Fig. 6. Comparison of predicted residual C_p with experimental residual C_p in the liquid region for the CO_2 + SO_2 mixture (95.03%). Experimental data (scatter points) are taken from [35]

Table 7
Mean absolute percentage error (MAPE) in predicted speed of sound of CO_2 + SO_2 mixture with reference to experimental data from [34]

Equation of state	Molar fraction	MAPE of speed of sound			
		−10 °C	0 °C	20°	31 °C
PR	80% CO_2	11.2%	10.5%	10.1%	10.3%
PC-SAFT		1.7%	1.6%	1.5%	1.5%
REFPROP		0.6%	0.7%	1.0%	1.2%

Table 8
Mean absolute percentage error (MAPE) in residual specific heat of CO_2 + SO_2 mixture with reference to experimental data from [35]

Equation of state	Molar fraction	MAPE of residual specific heat					
		400 bar	350 bar	300 bar	250 bar	200 bar	150 bar
PR	95%	7.3%	4.6%	4.1%	5.8%	7.5%	14.6%
PC-SAFT	CO_2	11.4%	4.7%	4.2%	3.8%	5.5%	13.7%
REFPROP		7.2%	1.4%	3.3%	8.5%	11.0%	17.1%

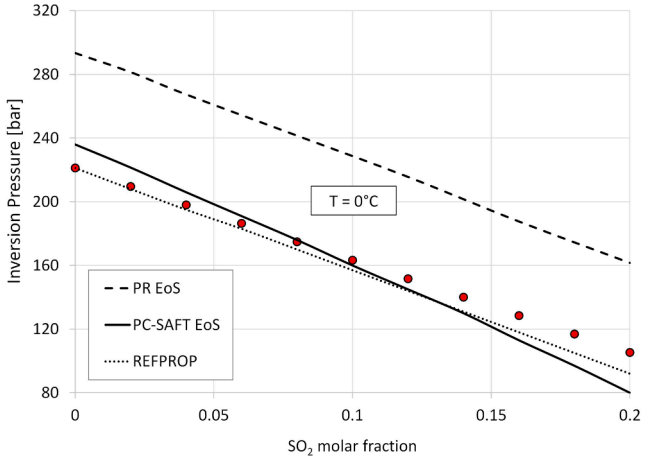

Fig. 7. Inversion curve at 0 °C for the CO_2 + SO_2 mixture at different molar composition. Experimental data shown by solid circles is taken from ref [34]

2.3. Identification of the most accurate EoS

The final scope of this section is to identify the most accurate EoS to be adopted for the techno-economic assessment of the CO_2 + SO_2 mixture used as working fluid in closed cycles. With respect to the approach adopted in literature, which uses only VLE data for the assessment of the most accurate EoS, the comparison is here extended also considering densities, specific heats and speeds of sound. For this reason the identification of the most suitable EoS is more challenging, since it can be difficult to combine MAPEs at different temperatures and compositions for different set of properties and select the most accurate EoS. Therefore, the properties of the mixture are divided into four categories: VLE, density, speed of sound and residual specific heat. A single MAPE indicator is computed for each set of property incorporating all the data points at different compositions, temperatures and pressures. Table 9 reports the overall MAPE for each category of experimental data fitted by the EoS, along with an average MAPE computed considering the four previous data.

Table 9
Overall MAPE in different set of thermodynamic properties.

EoS	MAPE				
	VLE	Density	Speed of sound	Residual C_P	Average
PR	1.1%	2.5%	10.4%	7.3%	5.3%
PC-SAFT	2.0%	1.4%	1.6%	7.2%	3.0%
REFPROP	1.5%	2.3%	0.9%	8.1%	3.2%

Table 10
Experimental uncertainties of the experimental data gathered for the analysis on this work.

u_{VLE} [33]	$u_{Density}$ [35]	$u_{Density}$ [34]	$u_{SoundSpeed}$ [34]
0.2%	0.2%	0.05%	0.06%

According to the analysis of this work, the PR EoS is discarded due to the poor capability of fitting some of the advanced calorimetric properties, while both the PC-SAFT and the REFPROP equations are evidenced as adequate models to be used for this mixture.

Considering the calculations of the PC-SAFT model on the densities and the overall accuracy along the whole analysis, this model is selected as the reference EoS for the remaining cycle calculations for this mixture: as a matter of fact, PC-SAFT is the EoS that presents the lowest average MAPE indicator, justifying its choice as selected model. Regarding the VLE calculations, it must be reminded that the different relative errors on these experimental data between the three models are computed with modified equations fitted on the VLE quantities themselves (through the BIP): the precision of these calculations represent an upper limit of the fitting capability for each adopted model.

Moreover, considering the magnitude of the MAPE computed, it is important to account for the actual experimental uncertainty of the experimental data: if the experimental uncertainty and the MAPE computed with the EoS on the experimental data are of the same magnitude, the comparison may be considered weak. Table 10 reports the average experimental uncertainty reported in the works of Coquelet [33], Gimeno [34] and Nazeri [35].

Being the experimental uncertainties an order of magnitude below the computed MAPE by the EoS, the comparison between EoS based on the fitting capability with experimental data can be considered valid.

In conclusion, using the selected PC-SAFT EoS, the global phase diagram of the mixture is computed and reported. It includes mixture critical points and P-T envelope at different molar compositions as illustrated in Fig. 8. The P-T envelopes allow to identify the critical point locus of the mixture, which is important for the selection of the mixture composition when the working fluid is used for transcritical cycles: as a matter of fact, the pump inlet of the cycle is expected to be placed near the bubble point conditions at a temperature lower than the critical one, for any composition of the mixture.

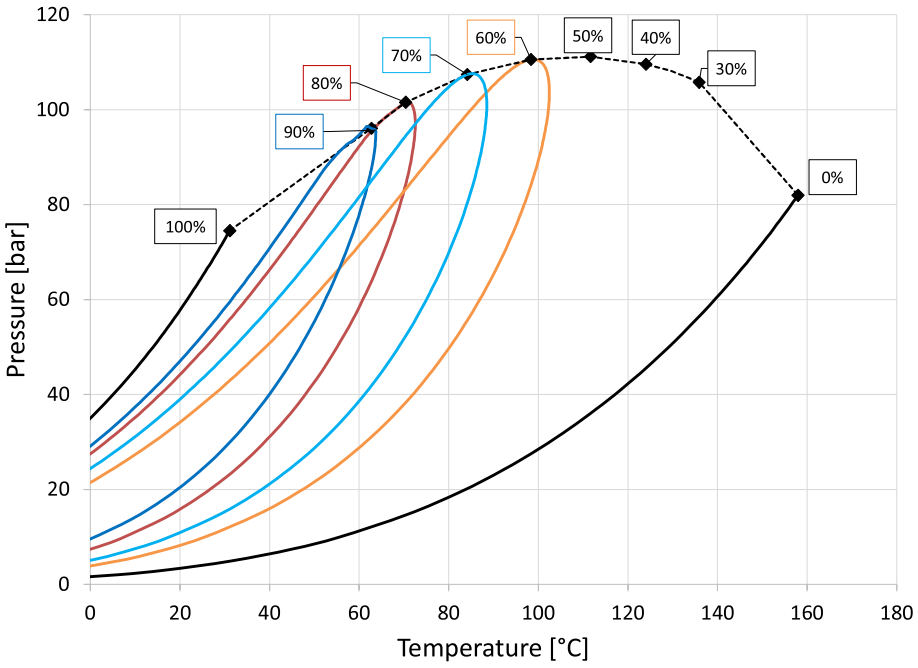

Fig. 8. P-T envelopes of the $CO_2 + SO_2$ mixture at various molar composition modelled with the PC-SAFT EoS. Rhombus points show the mixture critical points. The flags indicate the CO_2 molar content.

3. Techno-economic assessment methodology

After the selection of the most suitable equation of state for the mixture, this work analyses the potentiality of an innovative power block adopting the $CO_2 + SO_2$ mixture as working fluid and compares the performance of the cycle adopting the mixture against sCO_2 cycles. The authors considered the application of the innovative power cycle in CSP plants with advanced solar towers achieving a maximum temperature of the working fluid of 700 °C, as both sCO_2 and the $CO_2 + SO_2$ mixture are considered thermally stable at this temperature.

The comparison is performed in terms of both cycle performances and economic performances.

The methodology adopted for the technoeconomic assessment is the following:

- Identification of cycle layouts based on some typical configurations found in literature
- Thermodynamic analysis to assess the cycle performances
- Evaluation of cycle costs based on a bottom-up approach (i.e. sum of the single component costs)

Finally, the key performance indicators to compare the different cases are defined.

3.1. Cycle layouts

Different cycle layouts adopting the $CO_2 + SO_2$ mixture are considered and represented in Fig. 9. In this work, the same layouts are also adopted in pure sCO_2 cycles which are considered as reference cases. All the selected cycle layout are taken from a previous work on sCO_2 cycles [10].

The first layout, depicted in Fig. 9a, is the simple recuperative cycle: it is the simplest layout with the lowest number of cycle components (pump, recuperative heat exchanger, primary heat exchanger, turbine and heat rejection unit). The reheated cycle, shown Fig. 9b, is then considered as an option to increase the cycle efficiency by increasing the average temperature of heat introduction into the cycle. The precompression cycle proposed in Fig. 9c, instead, allows to expand the flow in the turbine to a pressure below the pump inlet pressure: in this layout the turbine outlet pressure is an optimization variable and the temperature difference across the PHE inevitably increases, thus requiring an additional compressor. Then, the recompression cycle depicted in Fig. 9d is considered in this analysis, since it is the most efficient between the ones studied for sCO_2 cycles and widely adopted in literature as a reference for CSP applications [37]. In addition to high efficiency cycle layouts, heat recovery layouts are also considered in this analysis: for this reason, the partial heating cycle, the dual recuperated cycle and the cascade cycle are modelled (case (e), (f) and (g) of Fig. 9, respectively). The partial heating cycle allows the introduction of heat directly after the compression step in a fraction of the overall working fluid, the dual recuperated cycle has the characteristic to preheat in a recuperator only a fraction of the working fluid before the admission of it into the PHE, while in the cascade cycle all the working fluid is preheated in a recuperator, before the flow is separated in the splitter.

Heat recovery cycles focus on the reduction of the inlet temperature at the PHE instead of increasing the cycle efficiency [38]: this can be a relevant aspect in CSP plants when a large thermal energy storage is employed and when the selected optimization strategy aims to achieve a substantial number of equivalent hours of the power plant.

3.2. Thermodynamic analysis

The cycles simulations are performed in this work using Aspen Plus v11. Within this environment, the PC-SAFT EoS for the $CO_2 + SO_2$ mixture and the Span and Wagner EoS for pure sCO_2 are adopted as explained in the previous section.

CO_2 molar fractions from 70% to 85% are considered for this mixture: in general, the calculation of the locus of critical points of the mixture (presented in Fig. 8) helps in the identification of the acceptable range of molar fractions. In fact, a molar CO_2 composition higher than 85% would not allow for the condensation of the working fluid in a cycle with the minimum temperature of 51 °C (as the pump inlet would be too close to the critical point), and a molar CO_2 composition below 70% would have a critical temperature too high. Moreover, limiting the dopant content is always preferable when considering CO_2-based mixtures with not friendly dopants. The cycle maximum pressure, assumed

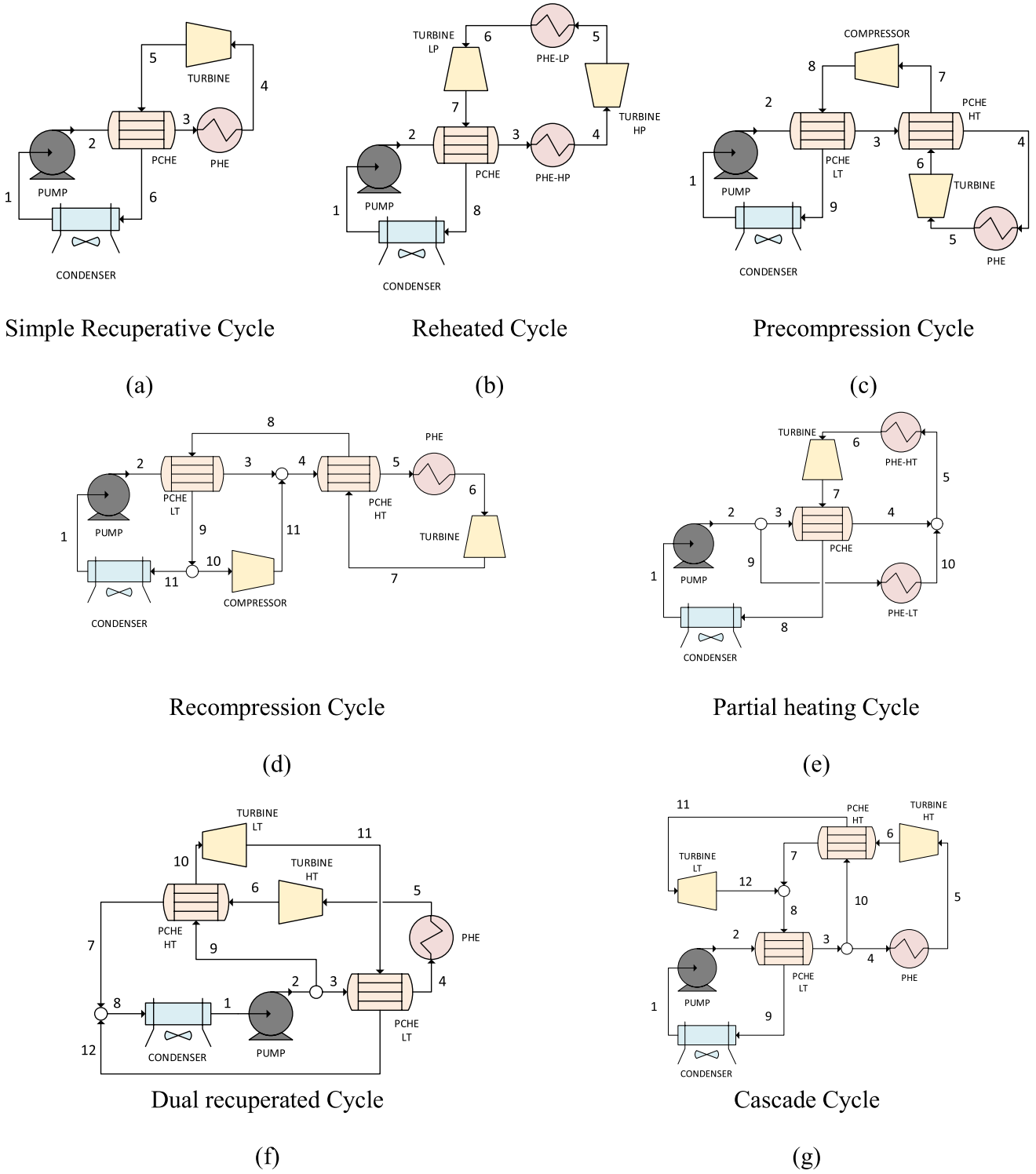

Fig. 9. Power cycle plant layouts proposed in this work.

as the pressure at the inlet of the turbine, is varied from 200 bar to 400 bar: it is worth noticing that maximum pressures of 250 bar are typical for these applications as they represent a technological limit.

The cycle maximum temperature is fixed at 700 °C in all the cases (both for the $CO_2 + SO_2$ mixture and pure CO_2). As anticipated, this temperature represents the target for the next generation CSP solar tower power plants. Moreover, in order to reproduce the hot and arid environments typical of CSP locations, a design ambient temperature of 35 °C is established and a corresponding minimum cycle temperature of 51 °C is set along the entire analysis [23]. The temperature differences at the cold end and hot end of the primary heat exchanger (PHE) are reported in Fig. 10 as function of the working fluid temperature at PHE inlet: the purpose of increasing the cold-end temperature difference in the PHE at lower temperature is to increase the ΔT_{ML} of the overall PHE, aiming at a reduction of power block cost. All the other assumptions on the non-idealities of the power cycle components are reported in Table 11.

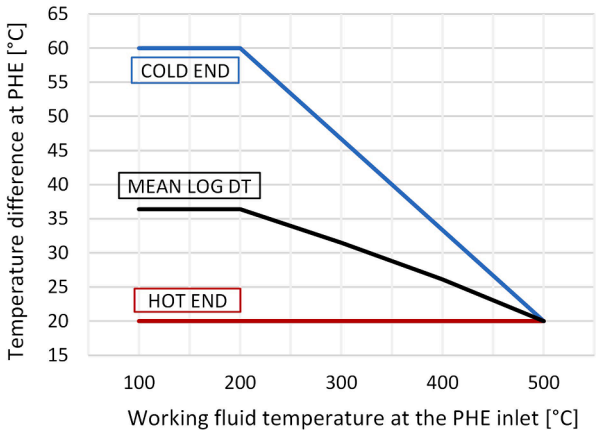

Fig. 10. Temperature difference on both sides of the PHE and respective PHE.ΔT_{ML}

Table 11
Assumptions on the power cycle performances.

Cycle minimum temperature	51 °C
Cycle maximum temperature	700 °C
Compression Isentropic efficiency	88%
Expansion Isentropic Efficiency	92%
MITA (Minimum Internal Temperature Approach) of PCHEs	5 °C
DP/P Main PHE	2%
DP/P Secondary PHE	2%
DP/P PCHE HP Side	0.3%
DP/P PCHE LP Side	1.5%
DP/P Condenser	2%
Expander electromechanical efficiency	98.7%
Pump/compressor electromechanical efficiency	97%
Air-cooled condenser auxiliary consumption	1.5% Q_{COND}

3.3. Key performance indicators

Various cycle components are modelled within this work: pumps, compressors, turbines, recuperators, PHE and condensers (or heat rejection units for the sCO_2 cycles). Under this perspective, turbines, pumps and compressors are characterized by their power, while heat exchangers by their thermal duty. The equations used to model the various cycle components are presented in Eq. (5) to Eq. (10):

$$\mathrm{Power_{Compression}} = \dot{m}_{\mathrm{compressed}} \cdot \left(h_{iso}^{\mathrm{outlet,compression}} - h^{\mathrm{inlet,compression}}\right) / \eta_{\mathrm{iso,compressor}} \quad (5)$$

$$\mathrm{Power_{Expansion}} = \dot{m}_{\mathrm{expanded}} \cdot \left(h^{\mathrm{inlet,expansion}} - h_{iso}^{\mathrm{outlet,expansion}}\right) \cdot \eta_{\mathrm{iso,expander}} \quad (6)$$

$$\mathrm{Q_{IN,PHE}} = \dot{m}_{\mathrm{PHE}} \cdot \left(h^{\mathrm{outlet,PHE}} - h^{\mathrm{inlet,PHE}}\right) \quad (7)$$

$$\mathrm{Q_{PCHE}} = \dot{m}_{\mathrm{PCHE,HP}} \cdot \left(h^{\mathrm{outlet,PCHEHP}} - h^{\mathrm{inlet,PCHEHP}}\right) = \dot{m}_{\mathrm{PCHE,LP}} \cdot \left(h^{\mathrm{inlet,PCHELP}} - h^{\mathrm{outlet,PCHELP}}\right) \quad (8)$$

$$\mathrm{Q_{Condenser}} = \dot{m}_{\mathrm{condensed}} \cdot \left(h^{\mathrm{inlet,condenser}} - h^{\mathrm{outlet,condenser}}\right) \quad (9)$$

$$\mathrm{UA_{PCHE}} = \frac{\mathrm{Q_{PCHE}}}{\Delta T_{\mathrm{ML,PCHE}}} \quad (10)$$

The thermodynamic analysis proposed aims at exploring the trend of four key performance parameters as descriptive of the overall thermodynamic cycle performance. They are the gross cycle efficiency, the cycle gross specific work, the temperature of the working fluid at the inlet of the PHE and the relative size of the recuperators.

Three of the four indicators are defined as reported in Eq. (11) to Eq. (13):

$$\eta_{cycle} = \frac{Power_{Expansion} - Power_{Compression}}{Q_{IN,PHE}} \quad (11)$$

$$w_{Specific,Cycle}[kJ/kg] = \frac{Power_{Expansion} - Power_{Compression}}{\dot{m}_{Cycle}} \quad (12)$$

$$UA_{PCHE}/Q_{IN}[1/K] = \frac{\sum UA_{PCHE,i}}{Q_{IN,Cycle}} \quad (13)$$

When defining the cycle efficiency, the power consumed or produced during the compression and expansion phase is considered as mechanical power, not including the electromechanical efficiencies of the turbomachinery, and $Q_{IN,PHE}$ is the thermal power introduced in the cycle by the hot source. Considering the gross cycle specific work, it is computed with respect to the mass flow rate $\dot{m}_{Compression}$ during the compression phase to make a consistent comparison between all the plant layouts, including the ones characterized by two turbines. The only exception being the recompression cycle, where two compression phases and only one expansion phase are present: in this case the specific work is computed with respect to the mass flow rate expanded $\dot{m}_{Expansion}$.

The relative size of the recuperators, UA_{PCHE}/Q_{IN}, accounts for each recuperator $UA_{PCHE,i}$ dimension parameter, computed by Aspen Plus with a 200 steps discretization of the heat exchanged domain.

Overall, the cycle efficiency is considered as the most important descriptor of a thermodynamic cycle: as a matter of fact, the sCO_2 cycle is renowned as an efficient cycle, especially in case of the recompression layout [10]. In solarized cycles the cycle efficiency directly determines the size of the solar field itself, and therefore it is strictly related to the specific CAPEX of the overall power plant and the LCOE. The cycle specific work is important in closed cycle since it accounts for: i) the overall working fluid inventory (generating an additional cost when non-conventional working fluids are considered), ii) the mass flow rate of the cycle itself (high mass flow rates increase the size of the cycle components and their cost), iii) the environmental impact of any leakage of the working fluid in case of leakages or damages. The third key performance parameter, the working fluid temperature at the inlet of the primary heat exchanger, is another crucial indicator of costs and thermodynamic performances in solarized cycle, since the lower the temperature of heat introduction, the higher the temperature difference of the HTF. In CSP plants, a high temperature differences of the HTF would result in: i) an increase of the receiver thermal efficiency, due to a corresponding reduction of thermal losses between the receiver and the environment, ii) a lower HTF flow rates at constant thermal input, thus reducing the size and cost of the TES. Nevertheless, following the trend of the Carnot efficiency, a lower temperature at the PHE inlet inevitably reduces the cycle efficiency. The last parameter, the relative size of the PCHE, expressed as UA_{PCHE}/Q_{IN}, accounts for the physical dimensions of the recuperators: since the various plant layouts present significant differences between each other, this parameter gives an indication of the recuperators size, and consequently their cost.

Table 12
Cost functions adopted in this work for the modelling of the CAPEX of CO_2-based power cycles.

Component	Cost Function [M$]	Reference
Turbine	$3.49 \cdot 182600 \cdot W[MW]^{0.5561}$	Weiland, 2019 [39]
Compressor/Pump	$1.23 \cdot W[MW]^{0.3992}$	Weiland, 2019 [39]
PCHE	$49.45 \cdot UA[MW/K]^{0.7544}$	Weiland, 2019 [39]
PHE	$3.5 \cdot UA[MW/K]$	Carlson, 2017 [40]
Condenser	$32.88 \cdot UA[MW/K]^{0.75}$	Weiland, 2019 [39]
Generator	$0.1089 \cdot W[MW]^{0.5463}$	Weiland, 2019 [39]
Motor	$0.3994 \cdot W[MW]^{0.606}$	Weiland, 2019 [39]
Fraction of Direct Costs	All components except PCHE: 20% PCHE: 5%	Weiland, 2019 [39]

3.4. Economic assumptions

In a typical CSP plant the fraction of the overall power plant CAPEX which accounts for the power block cost can vary between 15% and 30%, mainly depending on the TES dimensions and the power block efficiency. Moreover, the proposed mixture presents some interesting characteristics for which it can be adopted in various applications, not only in solarized cycles. For these reasons the power block CAPEX is investigated as crucial variable of interest. These costs are calculated with a bottom-up approach: starting from the equipment cost as sum of each component (i.e. pump, turbine, etc), the overall CAPEX is determined with an additional percentage to account for direct cost, such as labor cost and transportation cost. Among the various reference cost functions for supercritical CO_2 cycles available in literature, the work by Weiland *et* al [39] has been selected as, to the authors knowledge, it is one of the most updated and based on a detailed review of cost functions for sCO_2 power cycles considering data provided by real vendors. The single exception is represented by the PHE: since it is not possible to find a cost function based on the UA parameter in Weiland, which is necessary for this work, the cost function by Carlson *et* al [40] has been selected. A more conservative results are hence expected on the PHE side for this reason. Moreover, the cost function presented by Weiland for sCO_2 compressors is used in this work also for pumps, due to lack of established references for thermal turbomachinery working with highly compressible liquids slightly below the critical point. An overview of the cost functions adopted is presented in Table 12.

The economic performance indicator adopted is the power block CAPEX itself, as the integration of the power block in the CSP plant is beyond the scope of this work. In future works the integration of the cycle in the solar plant will be studied, as the identification of the optimal configuration requires a complete economic assessment which includes the LCOE calculation, which is the reference index for power production plants.

4. Results

4.1. Cycle performance varying the maximum pressure and the molar fraction

As a preliminary necessary step to properly present the thermodynamic results of the power block, a sensitivity analysis on the cycle maximum pressure and the choice of the mixture composition is proposed in order to identify the best cycle layout and mixture composition. From Figs. 11-14, the trend of performance indicators for both CO_2 + SO_2 mixture and sCO_2 cycles is illustrated for all the considered plant layouts.

Considering the results in Fig. 11 it can be observed that the adoption of the mixture in the simple recuperative layout and in the reheated layout does not provide significant improvements on the sCO_2 cycles from a cycle efficiency perspective.

The most significant improvement of the CO_2 + SO_2 mixture with respect to the sCO_2 cycle in terms of cycle gross efficiency occurs for the recompression layout, with an increase of 2.1% (overcoming the 50% threshold) assuming a maximum pressure of 250 bar. In addition, the temperature of heat introduction decreases by 40 °C, the relative size of the PCHE decreases by more than 20% and the specific work increases by more than 25%. Combining these four aspects, the overall thermodynamic analysis on the recompression cycle suggests that the adoption of the mixture, with respect to the sCO_2 configuration, would allow significant improvements in the technoeconomic performances of the power cycle and of the power plant in which the cycle is employed.

Similar considerations can be applied to the precompression layout: a 0.5% cycle efficiency growth, a 40% reduction of the PCHE size and a

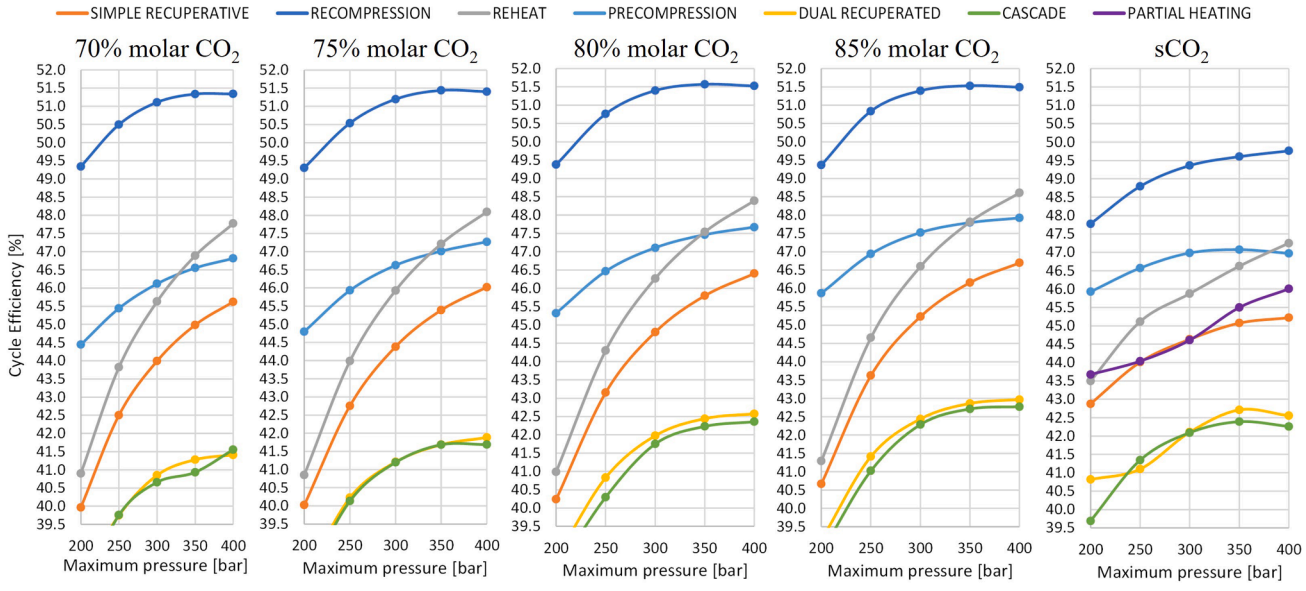

Fig. 11. Gross cycle efficiencies computed for the various plant layouts and various compositions of the working fluid considered.

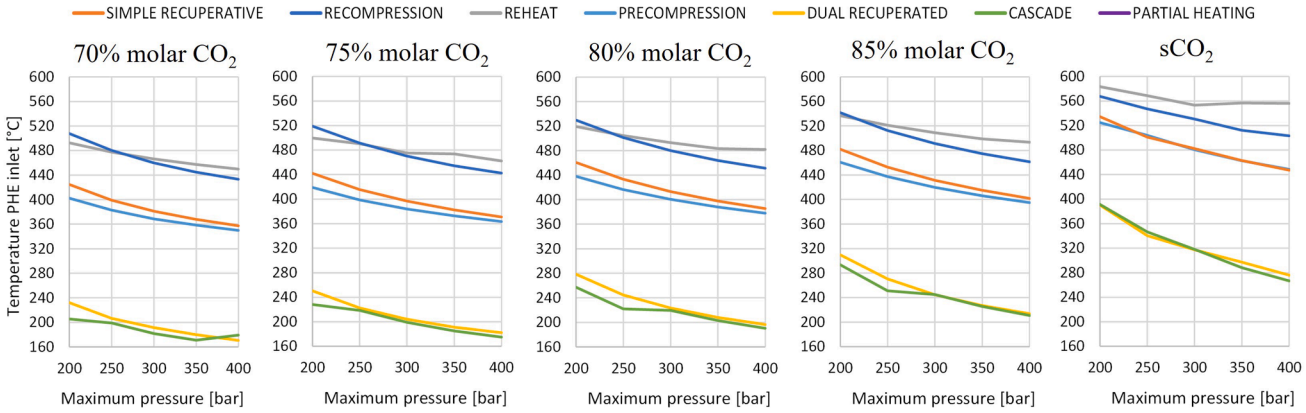

Fig. 12. Working fluid temperature at the inlet of the PHE for the various plant layouts and various compositions of the working fluid considered.

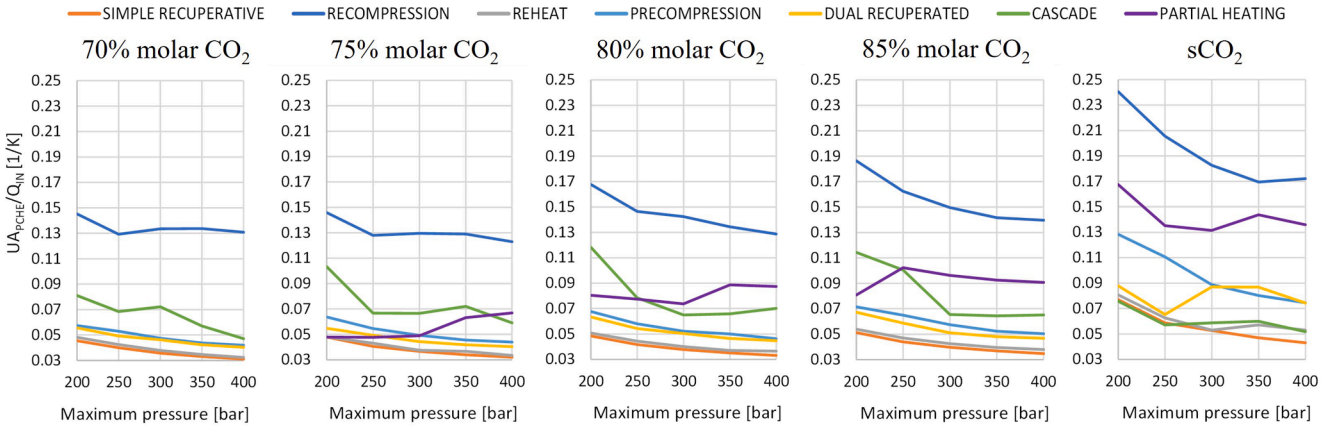

Fig. 13. Relative recuperators size of the power cycle for the various plant layouts and various compositions of the working fluid considered.

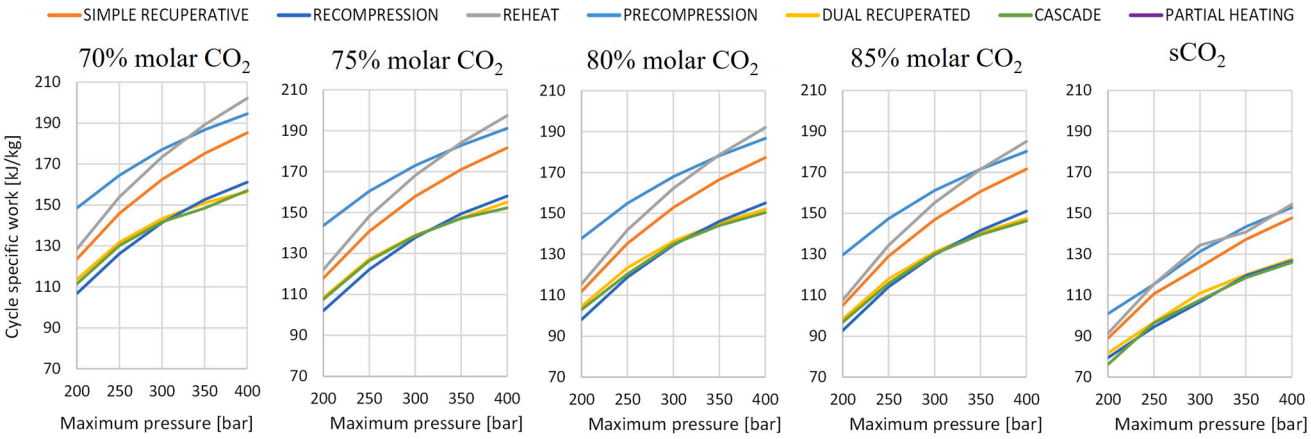

Fig. 14. Cycle gross specific work for the various plant layouts and various compositions of the working fluid considered.

25% growth of specific work with respect to pure sCO_2. Notably, the specific work of the precompression cycle is the highest between the various layout considered, since it is the only configuration where the expansion ratio of the turbine is higher than the pump compression ratio.

On the other hand, when it becomes necessary to decrease the temperature of the hot source, plant layouts from the heat recovery family can be also exploited (reported in Fig. 9(e, f and g)).

As a matter of fact, the previous analysis shows that the recompression cycle permits only a 150–200 °C of temperature difference of the working fluid in the PHE: in heat recovery cycle configurations, instead, this temperature difference is in the range of 420–480 °C, three times higher, as presented in Fig. 12.

The dual recuperated and the cascade cycle present comparable results in terms of cycle efficiency: depending on the layouts, these two heat recovery cycles achieve efficiencies between 41.0% and 41.5% for maximum pressures of 250 bar and between 42.0% and 42.5% for maximum pressures of 300 bar. The most considerable improvement

that the mixture can bring with respect to the pure sCO_2 cycle is in the heat introduction temperature, which can be up to 100 °C lower than the one of sCO_2 cycle, assuming the same heat recovery plant configuration. This difference can be mainly attributed to the lower temperature difference in the compression step of the transcritical cycle with respect to the compression of pure CO_2, that occurs in the supercritical phase.

The cycle efficiencies computed in various conditions of cycle maximum pressure also permits to identify the optimal mixture composition: under this perspective, the composition of the $CO_2 + SO_2$ mixture equal to 85% of CO_2 molar content is selected as the optimal one since it reaches the highest cycle efficiency in all configurations while, unfortunately, increases the recuperator relative sizes and reduces the specific work of the cycle. These last two characteristics are mainly caused by the trend of the mixture molar mass, which decreases at high CO_2 content and at low working fluid complexity.

The partial heating cycle presents some peculiarities, as the cycle efficiency of the transcritical cycle adopting this plant layout is the same as the simple recuperative one. This is mainly due to the position of the MITA in the recuperator: being the MITA on the cold end of the recuperator both in the partial heating cycle and in the recuperative cycle, the hot flow is cooled down as much as possible for the two cases. For this reason, in the condenser the same amount of heat is rejected from the cycle, and thus the cycle efficiency has the same exact value. Moreover, the cycle specific work is also coherent with the one calculated in the simple recuperative cycle, while the heat injection occurs in this layout starting from pump outlet: for these three reasons, most of the characteristics of the partial heating configuration are not reported in the graphical results.

4.2. *Cycle performance for a state-of-the-art power plant*

Once the comparison between the characteristics of sCO_2 cycles and transcritical $CO_2 + SO_2$ mixture cycles have been detailed in the previous chapter, a more detailed analysis is proposed focusing on the best efficient molar composition, considering a CO_2 molar fraction of 85% in the $CO_2 + SO_2$ mixture. In addition, the maximum pressure of the cycles is set at a state-of-the-art maximum value of 250 bar. Under these assumptions, the T-s diagrams of the power cycles considered are plotted in Fig. 15: these T-s diagrams allow for a comparison between the transcritical cycle working with the mixture and the sCO_2 cycle for each

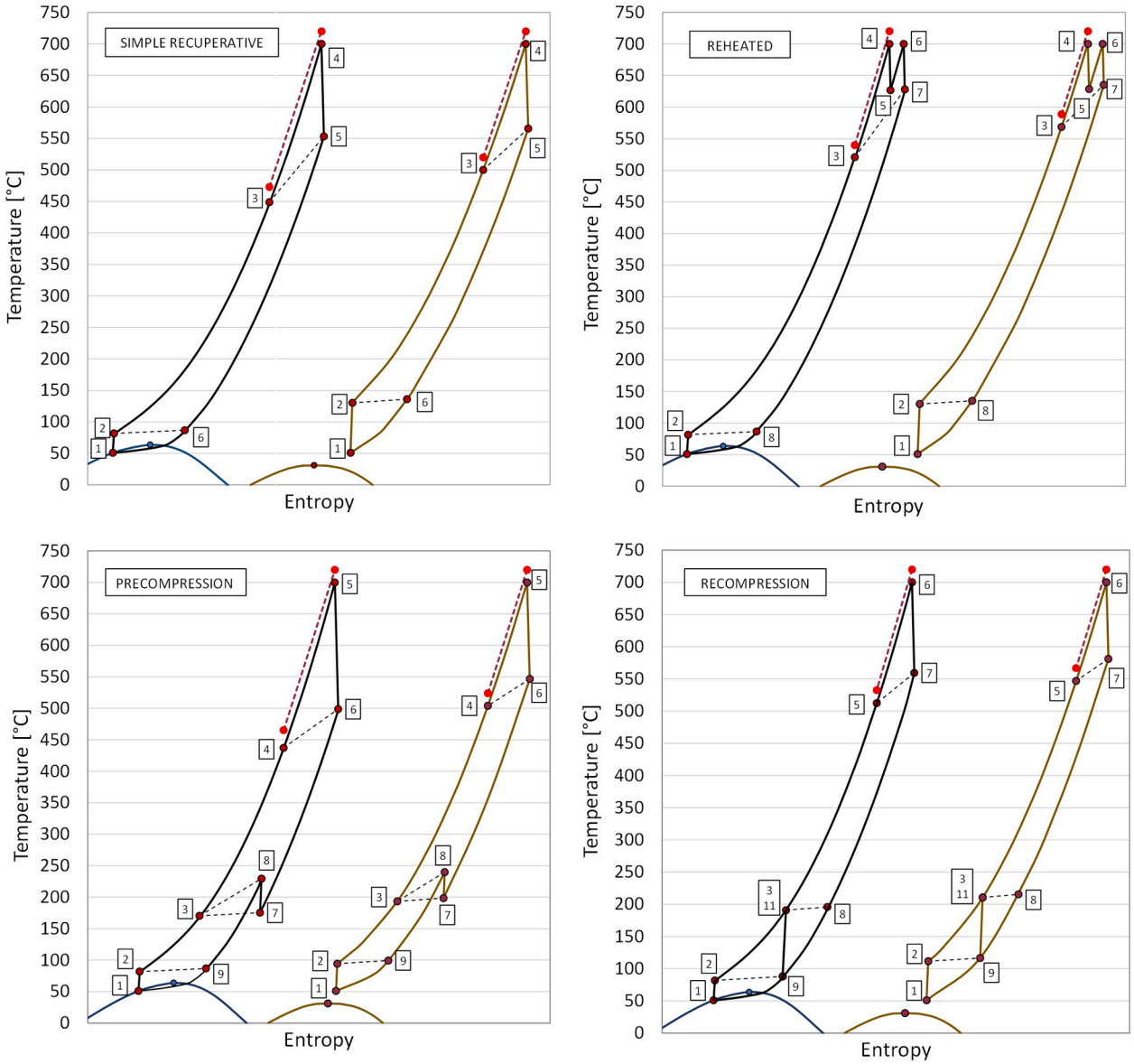

Fig. 15. T-s diagrams of the selected $CO_2 + SO_2$ mixture power cycles (left) and the respective sCO_2 cycles adopting the same plant layout (right). The dotted red lines represent the hot sources.

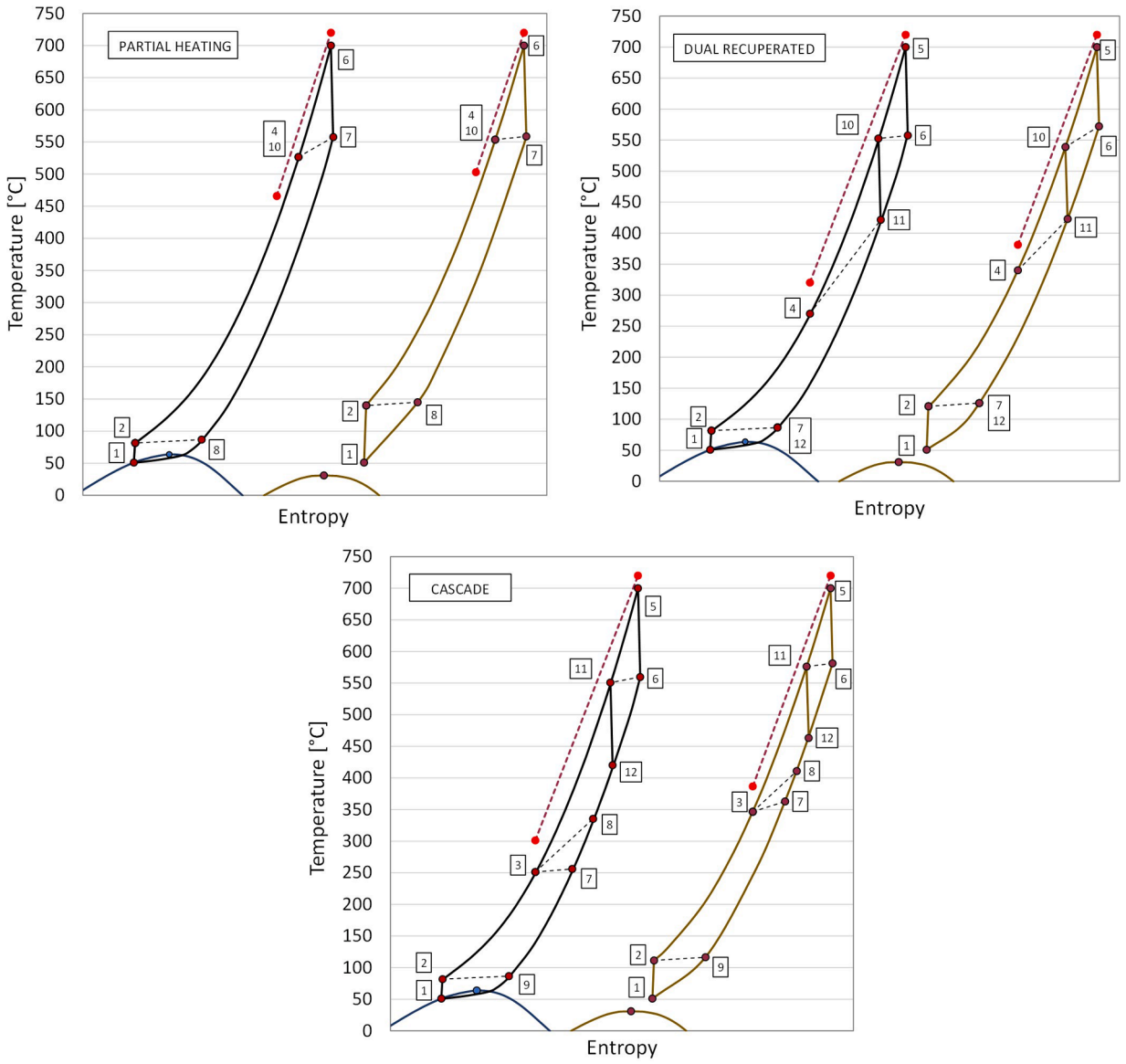

Fig. 15. (*continued*).

plant layout considered. In the diagrams the hot sources are also reported in order to illustrate the different heat introduction temperatures and the different cooling of the hot source for each configuration.

In addition to the T-s diagrams, the power balance of the power cycles is reported in Table 13 and Table 14 for the innovative cycles working with the mixture and the sCO_2 cycles, respectively: the results are shown assuming 100 MW as reference cycle gross power. The key performance indicators previously described are presented in the power balance, whereas the electromechanical losses and the auxiliary power consumed by the air cooled condenser are also modelled, accordingly to Table 11, in order to take into account the whole set of differences between the two working fluids: since supercritical sCO_2 cycles have a higher compression work than transcritical cycles, than higher electromechanical losses are computed. These two additional losses are indeed included in the calculation of the power block electric efficiency, presented in the power balance.

Considering these results, all cycle layouts adopting the transcritical configurations with the $CO_2 + SO_2$ mixture can achieve a higher net cycle efficiency than the respective sCO_2 cycles. Moreover, in case of CSP applications adopting solar towers, the net electric efficiency of the power plant would also account for the pump consumption for the HTF recirculation: this aspect is additionally beneficial for the configurations adopting the mixture, since all plant layouts experiences a higher temperature difference across the PHE and therefore a more limited mass flow rate of the HTF.

4.3. Economic analysis of the power block

A complete comparison between the innovative working fluid (the $CO_2 + SO_2$ mixture) and pure CO_2 used as working fluid in power cycles should also include some economic indicators. In this work, the capital cost of each power block configuration is analyzed, as descripted in Table 12. The results are presented accordingly in Fig. 16, considering a cycle net power of $100MW_{el}$, 250 bar as cycle maximum pressure and optimal composition for the mixture.

The adoption of the mixture always leads to a lower capital cost of the power block compared to the corresponding sCO_2 cycle configuration. Different reasons can explain this behavior: i) the compression of a supercritical fluid is a more energy intensive process than the one of a compressible liquid and therefore it brings to a higher cost of investment in the turbomachinery, ii) the mass flow rate flowing in sCO_2 cycles is higher than the respective transcritical counterpart working with the

Table 13
Performance of the power cycles working with the innovative $CO_2 + SO_2$ mixture under the assumptions of Table 12 and a maximum pressure of 250 bar.

	Transcritical $CO_2 + SO_2$ Cycle – 85% Molar CO_2 – P_{MAX} = 250 bar						
	Simple Recuperative	Reheated	Recompression	Precompression	Cascade	Partial heating	Dual recuperated
Cycle Efficiency [%]	43.62	44.66	50.84	46.94	41.02	43.62	41.41
Specific Work [kJ/kg]	129	134	114	147	116	129	118
UA_{PCHE}/Q_{IN} [1/K]	0.044	0.047	0.162	0.065	0.101	0.102	0.059
UA_{PHE} [MW/K]	9.32	11.4	9.17	8.49	7.3	11.78	7.40
T inlet PHE [°C]	453	521	513	437	251	–	270
Compression power [MW]	20.7	19.8	35.1	48.6	23.0	20.7	22.6
Expansion power [MW]	122.9	122.0	137.9	151.9	125.4	122.9	124.9
Heat rejected [MW]	132.1	126.6	99.5	116.7	147.1	132.2	144.8
Electro/mechanical losses [MW]	2.2	2.2	2.9	3.3	2.3	2.2	2.3
Heat rejection auxiliary [MW]	2	1.9	1.5	1.7	2.2	2	2.2
Power block electric efficiency [%]	41.81	43.87	48.67	44.65	39.22	41.81	39.58

Table 14
Performance of the sCO_2 power cycles under the assumptions of Table 12 and a maximum pressure of 250 bar.

	Supercritical CO_2 Cycle – P_{MAX} = 250 bar						
	Simple Recuperative	Reheated	Recompression	Precompression	Cascade	Partial heating	Dual recuperated
Cycle Efficiency [%]	44.01	45.11	48.79	46.57	41.34	44.04	41.10
Specific Work [kJ/kg]	111	115	95	115	97	112	97
UA_{PCHE}/Q_{IN} [1/K]	0.059	0.063	0.206	0.111	0.057	0.135	0.065
UA_{PHE} [MW/K]	11.7	11.3	10.6	11.2	8.6	11.75	8.6
T inlet PHE [°C]	501	569	547	504	347	–	340
Compression power [MW]	45.0	42.9	50.9	59.0	39.9	49.6	45.5
Expansion power [MW]	148.4	146.2	154.5	163.0	143.0	153.2	148.9
Heat rejected [MW]	131.4	125.6	108.7	119.2	146.3	131.5	148.1
Electro/mechanical losses [MW]	3.4	3.3	3.6	4	3.1	3.5	3.3
Heat rejection auxiliary [MW]	2.0	1.9	1.6	1.8	2.2	2.0	2.2
Power block electric efficiency [%]	41.75	42.88	46.34	44.00	39.20	41.69	38.89

mixture, due to the different specific works, iii) a lower relative size of the PCHE is generally computed in the cycles working with the mixture, cutting the recuperators cost, iv) the heat introduction temperatures of the sCO_2 cycles are always higher than the ones of the respective transcritical cycles, thus lower mean logarithmic temperature differences are experienced in the PHE, increasing the PHE size and cost. For these reasons the cycle components are negatively affected under a cost perspective when the sCO_2 cycle is compared to the transcritical $CO_2 + SO_2$ mixture cycle.

Moreover, to better focus on the possible reduction in power block specific costs, the economic analysis is presented in Fig. 17 for various power block sizes, presenting similar relative cost reduction for all sizes.

4.4. Focus on the two most promising plant layouts: The recompression and the dual recuperated cycle

While various plant layouts have been examined in the previous sections, only two applications for power cycles have been identified: the high efficiency cycles and cycles that aims at recovering heat from the hot source. In this last section the most promising configuration for each of these two categories have been selected and their results presented.

Due to its high gross cycle efficiency (over 50% in the configuration where the $CO_2 + SO_2$ mixture is adopted), the recompression layout is selected as representative of the first category, while the dual recuperated cycle is analyzed due to its low specific cost of the power block and

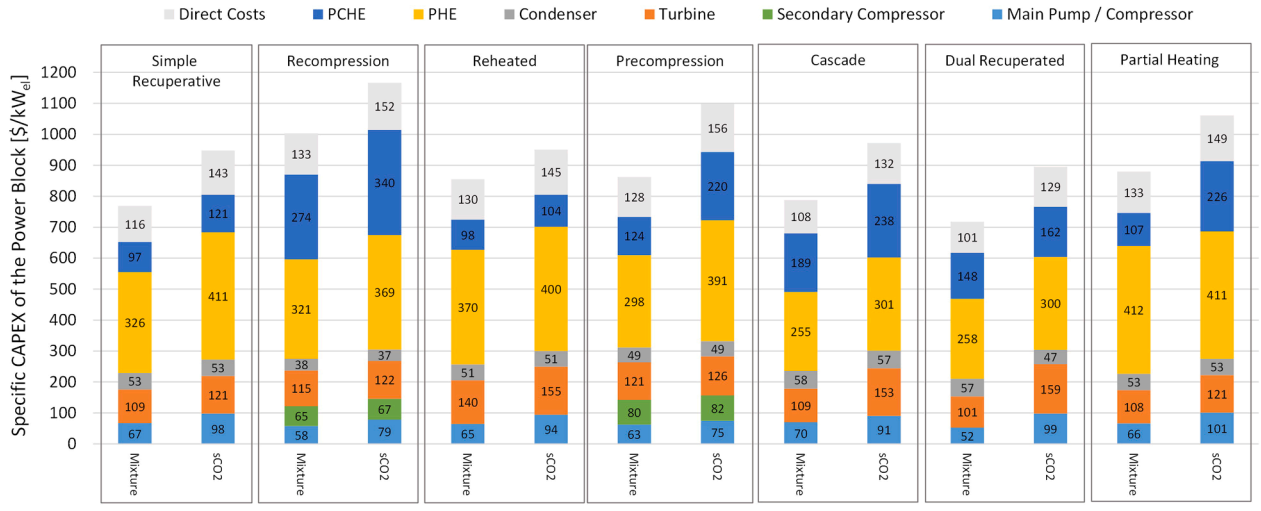

Fig. 16. Breakdown of the power block capital cost in all the plant layouts proposed for sCO_2 and $CO_2 + SO_2$ (85% CO_2 molar content) configurations. The calculations refer to 250 bar as maximum pressure and 100MW_{el} of cycle net power.

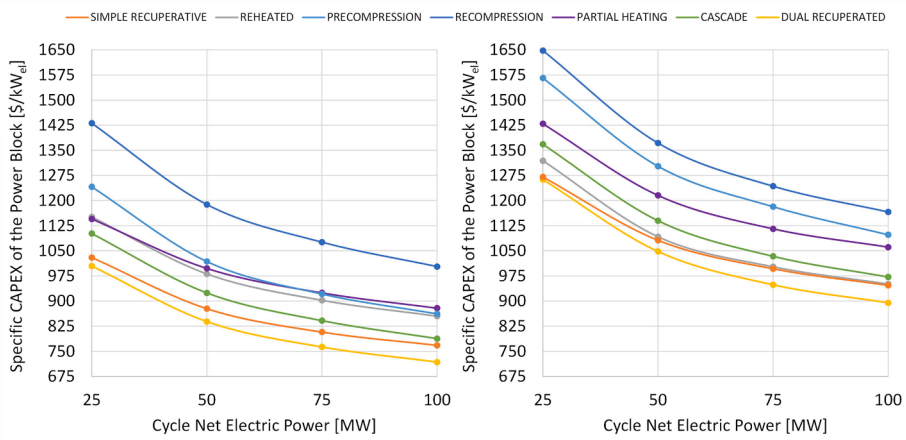

Fig. 17. Sensitivity analysis of the power block CAPEX for various cycle net electric powers: transcritical $CO_2 + SO_2$ (85% CO_2 molar content) cycle (left) and sCO_2 cycle (right).

the low heat introduction temperature. The last aspect is relevant for CSP plants where a high share of the power collected in the solar field is transferred to the thermal energy storage as well as for any other heat recovery applications exploiting high temperature heat.

The CAPEX breakdown of these two configurations is detailed and proposed in Fig. 18 and Fig. 19, respectively, for various molar compositions and maximum pressures: in general, the higher the SO_2 content in the mixture the higher the cycle specific work (as shown in Fig. 14) and thus a lower mass flow rate is needed for the cycle to meet the power target. For this reason, the lowest specific cost is computed when the SO_2 content is maximized. Moreover, higher maximum pressures favor higher cycle efficiencies and hence lower specific costs of the power block. Nevertheless, the range of maximum pressures reported in the figures is limited between 200 bar and 300 bar: any pressure higher than 300 bar is generally not considered in these applications and no consolidated cost functions for the high-pressure side components are available.

5. Conclusions

In this work a comparison between supercritical CO_2 power cycles and transcritical power cycles working with the $CO_2 + SO_2$ mixture is developed. The interest of this analysis lies in the identification and the thermodynamic description of an innovative mixture used as working fluid for closed power cycles operating in arid environment, where the cycle minimum temperature is above 50 °C, a condition that negatively affects the sCO_2 cycle performances. The analysis begins with a comprehensive collection of various experimental data from literature of the $CO_2 + SO_2$: data of densities, VLE, speed of sounds and residual heat capacities are compared with the calculated values by the Peng Robinson EoS, the PC-SAFT EoS and the embedded EoS in the software Refprop. In the second part of the paper, a complete thermodynamic analysis of the various power cycles is carried out, while the third section considers the economic analysis of the power block.

The outcomes of this work can be summarized as follows:

- The PC-SAFT EoS is assessed as a suitable and effective equation to properly model the thermodynamic behavior of the $CO_2 + SO_2$ mixture.
- Cycle simulations are proposed along with a wide selection of plant layouts that shows significant potentialities both in the most efficient power cycles and in heat recovery power cycle configurations. In almost all the configurations considered the heat introduction temperature of the innovative transcritical $CO_2 + SO_2$ cycle substantially decreases with respect to the respective sCO_2 configuration, the specific work increases, and the relative size of the recuperators decreases.
- From a cycle efficiency perspective, the recompression layout allows for the most significant improvement in thermodynamic performances with respect to sCO_2 cycles, while the dual recuperated

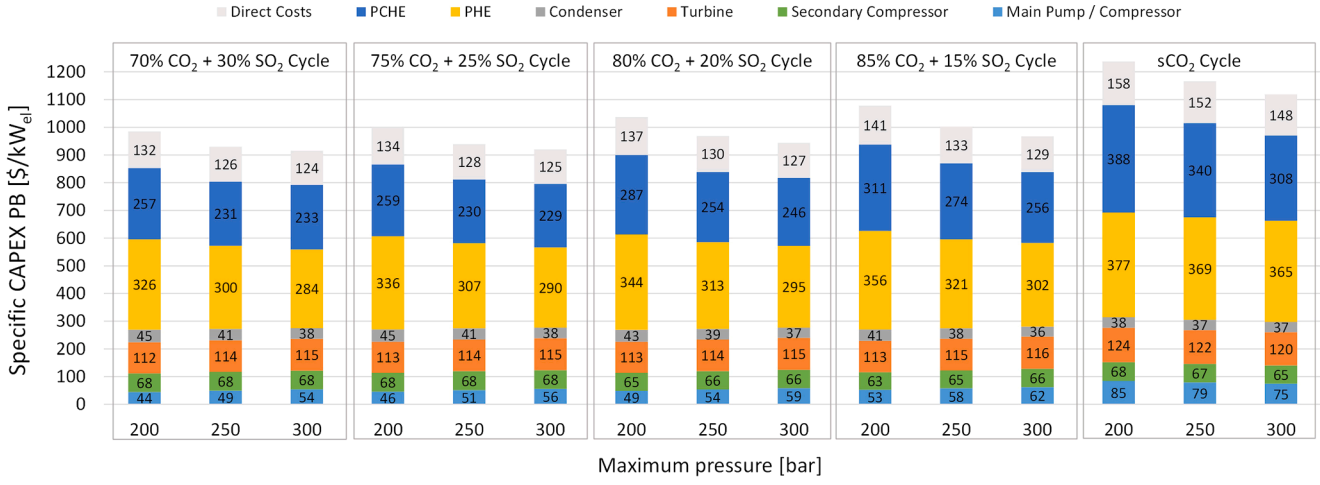

Fig. 18. Resulting power block CAPEX breakdown for the recompression plant layout at various working fluid compositions and cycle maximum pressures for a cycle net power of 100MW_{el}.

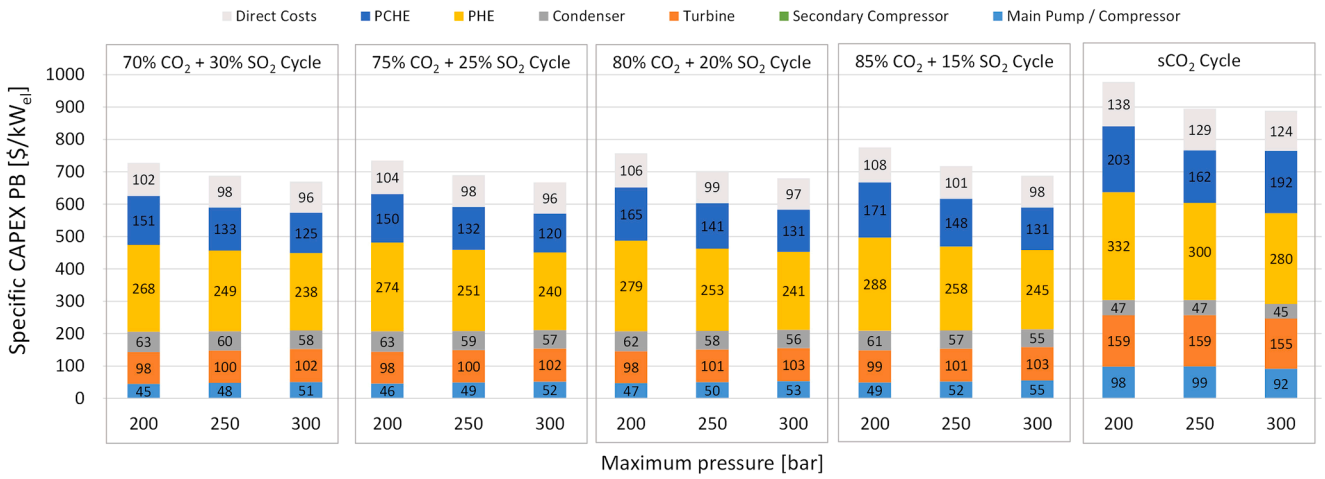

Fig. 19. Resulting power block CAPEX breakdown for the dual recuperated plant layout at various working fluid compositions and cycle maximum pressures for a cycle net power of 100MW_{el}.

layout is presented as the most appropriate one for heat recovery applications.

- In the recompression configuration, the adoption of the mixture allows for two percentage points increase in cycle efficiency (50.84% versus 48.79%) than the respective sCO_2 cycle with the same layout. Regarding the dual recuperated layout, comparable values of cycle efficiency are obtained, while a drop of 70 °C are obtained in the heat introduction temperature of the transcritical cycle with reference to the analogous sCO_2 cycle layout.
- Considering reasonable values for the electromechanical and auxiliary losses, the transcritical $CO_2 + SO_2$ cycles shows a higher net electric efficiency than the respective sCO_2 counterparts for a reference maximum pressure of 250 bar and a CO_2 molar fraction of 85%, for any cycle configuration considered.
- An economic analysis of the power block is carried out, using cost functions from the literature of sCO_2 cycles: the benefits of the transcritical configuration are confirmed from the economic perspective. Regarding the recompression cycle working with the optimal CO_2-SO_2 mixture a specific CAPEX of 1000 \$/kW_{el} is obtained, while a value of 1160 \$/kW_{el} is computed for the sCO_2 cycle with the same cycle layout. Similarly, the specific CAPEX of the dual recuperated cycle working with the optimal CO_2-SO_2 mixture is 718 \$/kW_{el}, an improvement when compared to the sCO_2 cycle in which the value is 795 \$/kW_{el} for the same cycle layout.

Considering the findings of this work, the $CO_2 + SO_2$ mixture is evidenced as a promising one for closed power cycles. Others important research fields for this innovative working fluid, different than CSP, can be also identified considering the high thermal stability of the mixture: for this reason, the application in high temperature heat recovery from exhaust gases (in the temperature range above 700 °C, like in the petrochemical, iron or steel industry [41]) can be beneficial from a technoeconomic perspective.

The major findings of this work can be nonetheless interpreted under a CSP perspective, where the higher fraction of the CAPEX (capital cost) is divided into solar field, thermal energy storage (TES) and power block costs.

Considering the operation of the power block in a CSP plant and assuming a constant net power output, a cycle efficiency increase from 48% to 50% (similar to the benefit that would bring adopting the recompression layout with the $CO_2 + SO_2$ mixture) leads to a reduction of the thermal power input by more than 4% which can be translated in a smaller heliostat field by the same amount (the most expensive part of the solar plant). Similarly, the thermal energy storage (TES) would also reduce its size by 4%, since a lower HTF inventory would be necessary to deliver the heat from the receiver or the TES to the power cycle. Therefore, the overall plant cost would reduce by around 4% in CAPEX which results into lower LCOE. On the other hand, the cycle efficiency is not the only important parameter: for example, a lower cycle heat introduction temperature would lead to a reduction in the TES specific cost, since a lower HTF flow rate would be necessary to transfer the same thermal power, and a much lower auxiliary consumption for the HTF circulation pump would be experienced.

For these reasons, depending on the applications of the innovative transcritical cycle, future works could analyze the integration of the power block with the solar power plant and the evaluation of the LCOE.

Declaration of Competing Interest

The authors declare that they have no known competing financial interests or personal relationships that could have appeared to influence the work reported in this paper.

Acknowledgements

This paper is part of the SCARABEUS project that has received funding from the European Union's Horizon 2020 research and innovation programme under grant agreement No 814985.

References

[1] T. International, R. Energy, and A. Irena, *RENEWABLE POWER GENERATION COSTS IN 2018*. 2018.
[2] Ortega JI, Burgaleta JI, Téllez FM. Central Receiver System Solar Power Plant Using Molten Salt as Heat Transfer Fluid. J. Sol. Energy Eng. May 2008;130(2): 0245011–6. https://doi.org/10.1115/1.2807210.
[3] Angelino G. Carbon Dioxide Condensation Cycles for Power Production. ASME J. Eng. Power 1968;90(3):287–96. https://doi.org/10.1115/1.3609190.
[4] White MT, Bianchi G, Chai L, Tassou SA, Sayma AI. Review of supercritical CO2 technologies and systems for power generation. Appl. Therm. Eng. Feb. 2021;185: 116447. https://doi.org/10.1016/j.applthermaleng.2020.116447.
[5] G. Manente and F. M. Fortuna, "Supercritical CO2 power cycles for waste heat recovery: A systematic comparison between traditional and novel layouts with dual expansion," *Energy Convers. Manag.*, vol. 197, no. July, p. 111777, Oct. 2019, 10.1016/j.enconman.2019.111777.
[6] S. A. Wright, C. S. Davidson, and W. O. Scammell, "Thermo-Economic Analysis of Four sCO2 Waste Heat Recovery Power Systems," *5th Int. Symp. – Supercrit. CO2 Power Cycles*, pp. 1–16, 2016.
[7] V. Dostal, M. J. Driscoll, and P. Hejzlar, "A Supercritical Carbon Dioxide Cycle for Next Generation Nuclear Reactors," *Tech. Rep. MIT-ANP-TR-100*, pp. 1–317, 2004, MIT-ANP-TR-100.
[8] U.S. Department of Energy, "Office of Energy Efficiency & Renewable Energy-The Sunshot Initiative." https://www.energy.gov/eere/solar/sunshot-initiative (accessed Jul. 27, 2021).

[9] L. Fang, Y. Li, X. Yang, and Z. Yang, "Analyses of Thermal Performance of Solar Power Tower Station Based on a Supercritical CO2 Brayton Cycle," *J. Energy Resour. Technol.*, vol. 142, no. 3, Mar. 2020, 10.1115/1.4045083.

[10] Crespi F, Gavagnin G, Sánchez D, Martínez GS. Supercritical carbon dioxide cycles for power generation: A review. Appl. Energy Jun. 2017;195:152–83. https://doi.org/10.1016/j.apenergy.2017.02.048.

[11] Khatoon S, Kim MH. Potential improvement and comparative assessment of supercritical Brayton cycles for arid climate. Energy Convers. Manag. 2019;vol. 200, no. June:112082. https://doi.org/10.1016/j.enconman.2019.112082.

[12] C. M. Invernizzi, "Prospects of mixtures as working fluids in real-gas Brayton cycles," *Energies*, vol. 10, no. 10, 2017, 10.3390/en10101649.

[13] Wang L, Pan L, Wang J, Chen D, Huang Y, Hu L. Investigation on the temperature sensitivity of the S-CO2 Brayton cycle efficiency. Energy Jul. 2019;178:739–50. https://doi.org/10.1016/j.energy.2019.04.100.

[14] Dai B, Li M, Ma Y. Thermodynamic analysis of carbon dioxide blends with low GWP (global warming potential) working fluids-based transcritical Rankine cycles for low-grade heat energy recovery. Energy 2014;64:942–52. https://doi.org/10.1016/j.energy.2013.11.019.

[15] Ayub A, Invernizzi CM, Di Marcoberardino G, Iora P, Manzolini G. Carbon Dioxide Mixtures as Working Fluid for High-Temperature Heat Recovery: A Thermodynamic Comparison with Transcritical Organic Rankine Cycles. Energies Aug. 2020;13(15):4014. https://doi.org/10.3390/en13154014.

[16] Jeong WS, Jeong YH. Performance of supercritical Brayton cycle using CO2-based binary mixture at varying critical points for SFR applications. Nucl. Eng. Des. 2013;262:12–20. https://doi.org/10.1016/j.nucengdes.2013.04.006.

[17] Liu X, Xu Z, Xie Y, Yang H. CO2-based mixture working fluids used for the dry-cooling supercritical Brayton cycle: Thermodynamic evaluation. Appl. Therm. Eng. Nov. 2019;162(17923):114226. https://doi.org/10.1016/j.applthermaleng.2019.114226.

[18] Guo JQ, Li MJ, Xu JL, Yan JJ, Wang K. Thermodynamic performance analysis of different supercritical Brayton cycles using CO2-based binary mixtures in the molten salt solar power tower systems. Energy 2019;173:785–98. https://doi.org/10.1016/j.energy.2019.02.008.

[19] S. Baik and J. I. Lee, "Preliminary study of supercritical CO2 mixed with gases for power cycle in warm environments," *ASME 2018 Turbo Expo*, pp. 1–8, 2018.

[20] S. Rath, E. Mickoleit, C. Breitkopf, and A. Jäger, "Study of the influence of additives to CO2 on the performance parameters of a sCO2-cycle," *4th Eur. sCO2 Conf. Energy Syst. March 23-24, 2021, Online Conf.*, pp. 212–229, Mar. 2021, 10.17185/DUEPUBLICO/73965.

[21] Manzolini G, Binotti M, Bonalumi D, Invernizzi C, Iora P. CO2 mixtures as innovative working fluid in power cycles applied to solar plants. Techno-economic assessment. Sol. Energy 2019;181(January):530–44. https://doi.org/10.1016/j.solener.2019.01.015.

[22] Bonalumi D, Lasala S, Macchi E. CO2-TiCl4 working fluid for high-temperature heat source power cycles and solar application. Renew. Energy Mar. 2020;147:2842–54. https://doi.org/10.1016/j.renene.2018.10.018.

[23] M. Binotti, C. M. Invernizzi, P. Iora, and G. Manzolini, "Dinitrogen tetroxide and carbon dioxide mixtures as working fluids in solar tower plants," *Sol. Energy*, vol. 181, no. September 2018, pp. 203–213, 2019, 10.1016/j.solener.2019.01.079.

[24] Di Marcoberardino G, Morosini E, Manzolini G. Preliminary investigation of the influence of equations of state on the performance of CO2 + C6F6 as innovative working fluid in transcritical cycles. Energy 2022;238:121815. https://doi.org/10.1016/j.energy.2021.121815.

[25] C. Craig, "Kirk-Othmer Encyclopedia of Chemical Technology and Ullmann's Encyclopedia of Industrial Chemistry," *Issues Sci. Technol. Librariansh.*, no. 46, p. 7, 2006, Accessed: Jun. 10, 2021. [Online]. Available: https://journals.library.ualberta.ca/istl/index.php/istl/article/view/2063.

[26] National Fire Protection Association, *NFPA 704 – Standard System for the Identification of the Hazards of Materials for Emergency Response*. 2007.

[27] Peng DY, Robinson DB. A New Two-Constant Equation of State. Ind. Eng. Chem. Fundam. 1976;15(1):59–64. https://doi.org/10.1021/i160057a011.

[28] Gross J, Sadowski G. Perturbed-chain SAFT: An equation of state based on a perturbation theory for chain molecules. Ind. Eng. Chem. Res. 2001;40(4):1244–60. https://doi.org/10.1021/ie0003887.

[29] Neumann T. Development of New Helmholtz Models for Binary Mixture Relevant for CCS. Ruhr-Universität Bochum; 2017.

[30] Løvseth SW, et al. Thermodynamics of the carbon dioxide plus argon (CO2 + Ar) system: An improved reference mixture model and measurements of vapor-liquid, vapor-solid, liquid-solid and vapor-liquid-solid phase equilibrium data at the temperatures 213–299 K and pressures up. Fluid Phase Equilib. 2018;466:48–78. https://doi.org/10.1016/j.fluid.2018.02.009.

[31] Span R, Wagner W. A New Equation of State for Carbon Dioxide Covering the Fluid Region from the Triple-Point Temperature to 1100 K at Pressures up to 800 MPa. J. Phys. Chem. Ref. Data 1996;25(6):1509–96. https://doi.org/10.1063/1.555991.

[32] Bertini M, Fiaschi D, Manfrida G, Niknam PH, Talluri L. Evaluation of the property methods for pure and mixture of CO2 for power cycles analysis. Energy Convers. Manag. 2021;245:114568. https://doi.org/10.1016/j.enconman.2021.114568.

[33] Coquelet C, Valtz A, Arpentinier P. Thermodynamic study of binary and ternary systems containing CO2+impurities in the context of CO2 transportation. Fluid Phase Equilib. Nov. 2014;382:205–11. https://doi.org/10.1016/j.fluid.2014.08.031.

[34] Gimeno B, Artal M, Velasco I, Fernández J, Blanco ST. Influence of SO2 on CO2 Transport by Pipeline for Carbon Capture and Storage Technology: Evaluation of CO2/SO2 Cocapture. Energy Fuels 2018;32(8):8641–57. https://doi.org/10.1021/acs.energyfuels.8b01666.

[35] Nazeri M, Chapoy A, Valtz A, Coquelet C, Tohidi B. New experimental density data and derived thermophysical properties of carbon dioxide – Sulphur dioxide binary mixture (CO2 – SO2) in gas, liquid and supercritical phases from 273 K to 353 K and at pressures up to 42 MPa. Fluid Phase Equilib. 2017;454:64–77. https://doi.org/10.1016/j.fluid.2017.09.014.

[36] "Aspen Plus | Leading Process Simulation Software | AspenTech." https://www.aspentech.com/en/products/engineering/aspen-plus.

[37] M. Mehos *et al.*, "Concentrating Solar Power Gen3 Demonstration Roadmap," *Nrel/Tp-5500-67464*, no. January, pp. 1–140, 2017, 10.2172/1338899.

[38] Zhao D, Zhao R, Deng S, Zhao L, Chen M. Transcritical carbon dioxide power cycle for waste heat recovery: A roadmap analysis from ideal cycle to real cycle with case implementation. Energy Convers. Manag. 2020;226:113578. https://doi.org/10.1016/J.ENCONMAN.2020.113578.

[39] N. T. Weiland, B. W. Lance, and S. R. Pidaparti, "SCO2 power cycle component cost correlations from DOE data spanning multiple scales and applications," in *Proceedings of the ASME Turbo Expo*, 2019, vol. 9, 10.1115/GT2019-90493.

[40] M. D. Carlson, B. M. Middleton, and C. K. Ho, "Cycles Using Component Cost Models Baselined With Vendor Data," *Proc. ASME 2017 Power Energy Conf.*, pp. 1–7, 2017.

[41] Bianchi G, Panayiotou GP, Aresti L, Kalogirou SA, Florides GA, Tsamos K, et al. "Estimating the waste heat recovery in the European Union Industry", *Energy*. Ecol. Environ. 2019;4(5):211–21. https://doi.org/10.1007/s40974-019-00132-7.